Performance Verification of Large Area Silicon Strip Sensors for GLAST

（ガンマ線衛星 GLAST 搭載大面積シリコン
ストリップセンサーの性能特性評価）

Hiroyuki Masuda

High-Energy Astrophysics and
Particle Physics (Experiment) Laboratory
Department of Physical science
Graduate school of science, Hiroshima University

February 8, 2002

広島大学大学院 理学研究科 物理科学専攻
高エネルギー宇宙・素粒子実験研究室
M1279024　増田 博之

Performance Verification of Large Area Silicon Strip Sensors for GLAST

Hiroyuki Masuda

High-Energy Astrophysics and
Particle Physics (Experiment) Laboratory
Department of Physical science
Graduate school of science, Hiroshima University

February 8, 2002

Abstract

We have investigated the performance and quality of pre-produced Flight Model (FM) silicon-strip-sensors for GLAST gamma-ray satellite. The leakage current, full depletion voltage, faulted strips and the effects of the gamma-ray irradiation on the sensors is investigated and we have confirmed that those results satisfy the specification for GLAST mission. For the mass produced sensors full depletion voltage, leakage current and faulted strips are investigated. In addition to these measurements, we sampled one test sensor from every production lot of about 30 full size sensors and investigated the effects of radiation damage of sensors as means to monitor the quality of fabrication process.

The leakage current density of these sensors is about 2nA/cm^2 at 25℃. This value is comparable to a low-leakage current photodiode. Such a low-leakage current enables us to screen out a sensor having few noisy strips instead of measuring individual strip current. This kind of low-leakage current sensor did not exist before. Thus we investigated the radiation damage of low-leakage current sensor because there might be unknown phenomena. First of all, we investigated the relation between the gamma-ray dose and increase of the leakage current. The leakage current of the irradiated sensor increases as the 0.8th power of dose. We also investigated the effect of the bias voltage to the sensor during and after the irradiation. The leakage current significantly differed whether the bias voltage was applied during the irradiation or not. The ultimate value of the leakage current of the former is about twice as large as that of the latter. There is an effect which softens the radiation damage (annealing effect) when the bias voltage is applying to the post-irradiated sensor which were not applied the bias voltage during the irradiation. Moreover, if we applied the bias voltage earlier after the irradiation, the effect is larger.

Contents

Chapter 1
Introduction

1-1. Gamma-ray Astrophysics

X-ray and gamma-ray space telescope satellites have revealed that the high-energy phenomena occur everywhere in the space since the gamma-ray object was first discovered. It means AGN (Active Galactic Nuclei), black hole candidate, particle acceleration to high energy and jet related to pulsar, the existence and the structure of shock front around the SNR (Super Novae Remnant), the existence of a large amount of the gas shut in the galaxy and galaxy cluster, gamma-ray burst and so on. In these objects, particles are accelerated very dynamically in various mechanisms, and the resulting high-energy particles are scattered into the cosmic space. It's just like a natural gigantic accelerator. In order to solve the high-energy phenomena in the hurt of and around the natural accelerators, it's essentially important to observe such astronomical phenomena in the gamma-ray band.

The scale of the gigantic accelerators in the space is really various, from the supernovae remnant (SNR) and active galactic nuclei (AGN) to gamma-ray burst, in examples. Owing to the development of the latest high-energy astrophysics, however, it has turned out that the high-energy particles accelerated by these space accelerators radiate the intrinsic gravity energy into the cosmic space in the form of the kinetic energy of the particles. What mechanisms works to radiate the energy which come in dozens of percent of rest mass $E = mc^2$ into the cosmic space at a high degree of efficiency in the forms of high-energy particles and radiation? Where are the ion and electron sources before acceleration? What is the mechanism of the particle acceleration? Is the cosmic ray, which flies about space, accelerated anywhere in these space accelerators? To answer to these questions, precise and systematic high-energy gamma-ray observation is needed.

The important interactions in observational study of gamma-ray astrophysics are really various. For examples, synchrotron radiation due to the interaction of high-energy electrons or protons and magnetic field, nonthermal bremsstrahlung from high-energy electrons, inverse compton irradiation due to the interaction of high-energy electron and photon, line gamma-ray irradiation accompanied with collapse of π^0 meson occurred by irradiation of cosmic-ray proton and nucleon and so on. Among these interactions, electron synchrotron is also used as a probe of high-energy astrophysics study in X-ray observations until now, but others are different from X-ray observations in quality and can be said that they are the probe peculiar to the gamma-ray region. Gamma-ray region is really most suitable for the study of space accelerators. Performing gamma ray observation with high accuracy systematically will mark a new epoch of high-energy astrophysics. [1]

1-2. GLAST Mission

GLAST Mission is part of NASA's Office of Space and Science Strategic Plan, with launch anticipated in 2006. GLAST is a next generation high-energy gamma-ray observatory designed for making observations of celestial gamma-ray sources in the energy band extending from 20 MeV to more than 300 GeV. It follows in the footsteps of the CGRO-EGRET experiment, which was operational between 1991-1999.

The key scientific objectives of the GLAST mission are:

1. **To understand the mechanisms of particle acceleration in AGNs*, pulsars*, and SNRs*.** This understanding is a key to solving the mysteries of the formation of jets, the extraction of rotational energy from spinning neutron stars, and the dynamics of shocks in SNRs.
2. **Resolve the gamma-ray sky: unidentified sources* and diffuse emission*.** Interstellar emission from the Milky Way and a large number of unidentified sources are prominent features of the gamma-ray sky.
3. **Determine the high-energy behavior of gamma-ray bursts* and transients.** Variability has long been a powerful method to decipher the workings of objects in the Universe on all scales. Variability is a central feature of the gamma-ray sky.
4. **Probe dark matter and early Universe.** Observations of gamma-ray AGN serve to probe supermassive black holes through jet formation and evolution studies, and provide constraints on the star-formation rate at early epochs through $\gamma\gamma$ absorption over extragalactic distances. There are also the possibilities of observing monoenergetic gamma-ray "lines" above 30 GeV from supersymmetric dark matter interaction; detecting decays of relics from the very early Universe, such as cosmic

strings or evaporating primordial black holes; or even using gamma-ray bursts to detect quantum gravity effects.

GLAST has a field of view about twice as wide (greater than 2.5 steradians), and sensitivity about 50 times that of EGRET at 100 MeV and even more at higher energies. Its two year limit for source detection in an all-sky survey is 1.6×10^{-9} photons cm^{-2} s^{-1} (at energies> 100 MeV). It will be able to locate sources to positional accuracies of 30 arc seconds to 5 arc minutes. Yet, it is a relatively small and inexpensive mission, which will be able to be launched on a Delta II rocket. [2]

＊ note

AGN (Active Galactic Nuclei) :

A class of galaxies which spew massive amounts of energy from their centers, far more than ordinary galaxies. Many astronomers believe supermassive black holes lie at the center of these galaxies and power their explosive energy output.

Pulsar :

Pulsars are rotating neutron stars. Pulsars were first discovered in late 1967 by Jocelyn Bell Burnell as radio sources that blink on and off at a constant frequency. Now we observe the brightest ones at almost every wavelength of light. Pulsars are spinning neutron stars that have jets of particles moving at the speed of light streaming out their two magnetic poles. These jets produce very powerful beams of light. For a similar reason that "true north" and "magnetic north" are different on Earth, the magnetic and rotational axes of a pulsar are also misaligned. Therefore, the beam of light from the jet sweeps around as the pulsar rotates, just as the spotlight in a lighthouse does. Like a ship in the ocean that sees only regular flashes of light, we see pulsars turn on and off as the beam sweeps over the Earth. Neutron stars for which we see such pulses are called "pulsars".

SNR (Super Novae Remnants) :

When a star explodes in a supernova explosion, it depends on its type what exactly remains. But anyway, the offbursted gaseous remainders will form a rapidly expanding and slowly fading cloud, mixing with the interstellar matter which is "swept up" when the shell expands, and is a domain of an extreme kind of physics. These nebulae are called supernova remnants (SNRs).

Unidentified sources :

More than 60% of the observed high-energy gamma-ray sources are unidentified. 170 of the271 sources in the Third EGRET Catalog still have yet to been identified. Possible candidates for these sources include active galactic nuclei , pulsars , supernova remnants , dense molecular clouds , and stellar-mass black holes within our Galaxy. It is even quite possible that entirely new phenomena could account for some portion of these unidentified sources.

Diffuse emission :

Non-point source gamma-ray emission from the plane of the galaxy. Mostly due to interactions of cosmic rays with interstellar materials.

Gamma-ray bursts :

Gamma-ray bursts (GRBs) pose one of the greatest mysteries of modern astronomy. About once a day, the sky lights up with a spectacular flash, or burst, of gamma-rays. More often than not, this burst out shines all of the other sources of cosmic gamma-rays added together. The source of the burst then disappears altogether. No one can predict when the next burst will occur or from what direction in the sky it will come. At present, we don't even know what causes these flashes or how far away they are.

1-3. GLAST's Instrumentation

The primary instrument required for the GLAST mission is an imaging, wide field-of-view telescope (the Large Area Telescope, or LAT) that covers the energy range from 20MeV to 300GeV. The two characteristics that the LAT will measure for each incoming gamma-ray are the energy of the photon and the angle at which the light ray hits the detector. These measurements will enable scientists to determine the location on the sky that produced the gamma-ray and the energy contained in that gamma-ray. The telescope consists of a tracker, followed by an energy-measuring calorimeter. The entire telescope is surrounded by anti-coincidence shielding, in order to eliminate signals which might be generated by background particles, such as cosmic rays. When a gamma-ray comes in contact with the converter material, it interacts to create a electron and positron pair. This interaction is called pair production. Each electron and positron then travels through the subsequent layers of tracking detectors and converters. For very energetic particles, further interactions occur, which produce additional pairs. The tracking detectors record information about the paths taken by the particles that are generated in the shower. On-board analysis of the tracker and calorimeter data provides initial information about the energy and direction of the shower and helps filter out additional background signals. The on-board triggering system will reject over 100,000 background signals for each gamma-ray photon that it identifies. The remaining signals are telemetered to the ground where they are further processed to determine the energy and direction of the gamma-ray photon. [2]

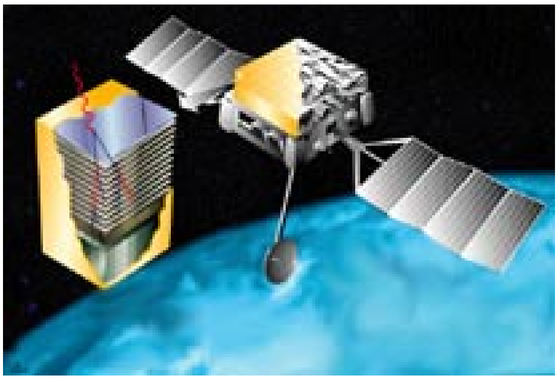

Fig 1-1. GLAST LAT.

LAT Silicon strip Detectors (SSDs)

The GLAST Large Area Telescope consists of a four-by-four array of tower modules. Each tower module consists of 16 interleaved pairs of silicon strip detectors and tungsten converter sheets, and an additional two pairs of silicon strip detectors without converters. Silicon strip detectors(SSDs) are able to more precisely track the electron or positron produced from the initial gamma-ray than previous types of detectors. SSDs will have the ability to determine the location of an object in the sky to within 0.5 to 5 arc minutes.

In each pair of silicon strip detectors, there are two planes of silicon, one plane has the strips oriented in the "x-direction", while the other has the strips oriented in the perpendicular "y-direction". When a particle interacts in the silicon, its position on the plane can therefore be determined in two dimensions. The third dimension of the track is determined by analyzing signals from adjacent planes, as the particle travels down through the telescope toward the calorimeter.

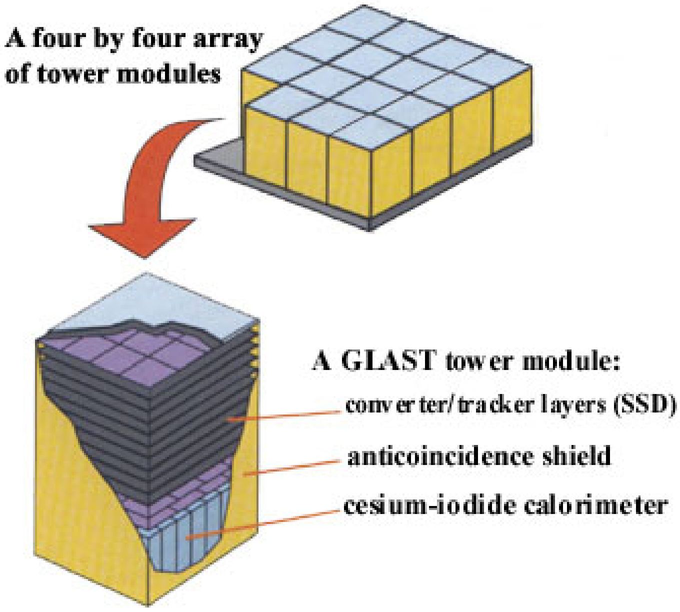

Fig 1-2. GLAST tower

LAT Cesium-Iodide Calorimeter

A calorimeter ("calorie-meter") is a device that measures the energy (heat in calories) of a particle when it is totally absorbed. Once a gamma-ray penetrates through the anticoincidence shield, the silicon strip tracker and tungsten converter planes, it then passes into the cesium-iodide calorimeters. This causes a scintillation reaction in the cesium-iodide, and the resultant light flash is photoelectrically converted to the charge signal with the photo-diode. This charge signal is then digitized, recorded and relayed to earth by the spacecraft's onboard computer and telemetry antenna. Cesium-iodide blocks are arranged in two perpendicular directions, to prove additional positional information about the shower.

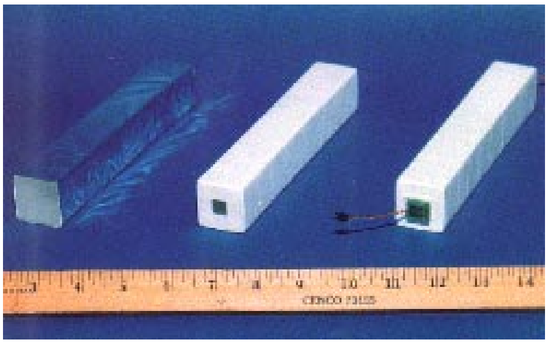

Fig 1-3. Calorimeter

LAT On-board Processor

The data acquisition system (DAQ) is the brain behind the GLAST, as it makes the initial distinction between false signals and real gamma-ray signals, and decides which of the signals should be telemetered to the ground. The DAQ consists of specialized electronics and 32-bit radiation-hard processors that record and analyze the information generated by the silicon strip detectors and the calorimeter. The DAQ will be shielded from the incredible rigors of space-flight, such as extreme high and low temperatures as well as high energy cosmic rays, which can cause the electronics to malfunction.

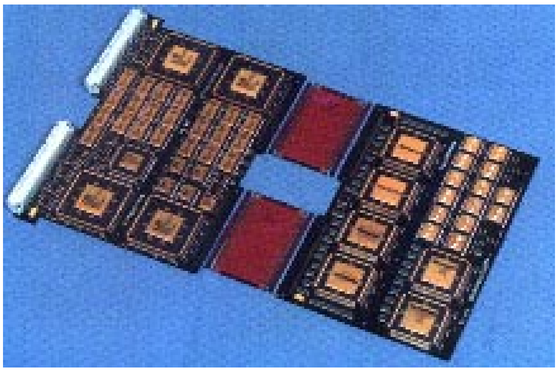

Fig 1-4. LAT On-board Processor

Quantity	EGRET	GLAST Requirement	GLAST Goal
Energy Range	20MeV−30GeV	20MeV−300GeV	10MeV−>300GeV
Effective Area (Peak)	1500 cm^2	8000 cm^2	>10,000 cm^2
Field of View	0.5 sr	2 sr	> 3 sr
Single Photon Angular Res. (68% containment angle)	5.8 ° (100MeV)	< 3.5 ° (100MeV) < 0.15 ° (> 10GeV)	2 ° (100MeV)
Energy Resolution	10%	10%	2% (> 10GeV)
Deadtime per Photon	100 μs	< 100 μs	< 20 μs
Source location Determination	5 ′ − 30 ′	1 ′ − 5 ′	30 ″ − 5 ′
Point Source Sensitivity (> 100 MeV)	$\sim 1\times10^{-7}$ $cm^{-2}s^{-1}$	4×10^{-9} $cm^{-2}s^{-1}$ (2-yr sky survey)	$< 2\times10^{-9} cm^{-2}s^{-1}$
Mass (instrument only)	1820 kg	3000 kg	
Power (instrument only)	160 W	650 W	
Orbit (28.5 ° incl.)	350 km	550 km	
Lifetime	1991−1999	2006−2011	2006−2016

Table 1-1. Abbreviated Listing of GLAST Specifications

Chapter 2.
Silicon Strip Sensor

2-1. Semiconductor

Materials can be categorized into conductors, semiconductors or insulators by their ability to conduct electricity. It is a popular belief that insulators do not conduct electricity because their valence electrons are not free to wander throughout the material. In fact they are free to move around, however, in an insulator there are as many electrons as there are energy levels for them to occupy. If an electron swaps place with another electron no change is made since electrons are indistinguishable. There are higher energy levels, but to promote the electrons to such a high energy levels requires an enormous voltage. Metals conduct electricity easily. In this case, the energy levels between the conduction and valence band are closely spaced and there are more levels than electrons so very little energy is required to find new energies for electrons to occupy. The resistivity of a material is measure of how difficult it is for a current to flow. Semiconductors have a resistivity between $10^{-4} < \rho < 10^{8}$ Ohms m although these are rough limits. The band theory of materials explains qualitatively the difference between these types of materials. Electrons occupy energy levels from the lowest energies upwards. However, some energy levels are forbidden because of the wave like properties of atoms in the material. The allowed energy levels tend to form bands. The highest filled level at T=0 is known as the valence band. Electrons in the valence band do not participate in the conduction process. The first unfilled level above the valence band is known as the conduction band. In metals, there is no forbidden gap; the conduction band and the valence band overlap, allowing free electrons to participate in the conduction process. Insulators have an energy gap that is far greater than the thermal energy of the electron, while semiconductor materials the energy gap is typically around 1eV. The diagram below summarizes the energy band model of materials.

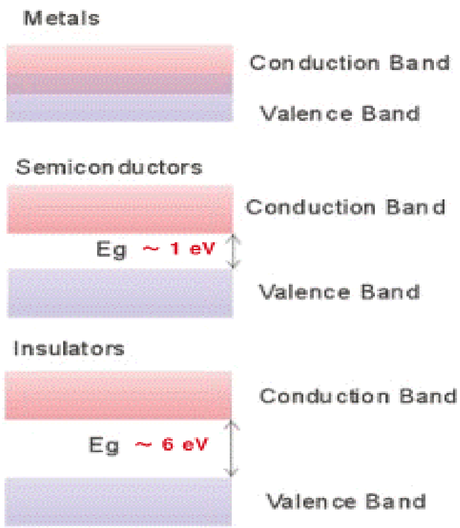

Fig 2-1. Basic energy band structure of conductors, semiconductors and insulators

― Intrinsic Semiconductors ―

Ideal intrinsic semiconductors are essentially pure semiconductor materials. The semiconductor material structure should contain no impurity atoms. At room temperature, the thermal energy of the atoms may allow a small number of the electrons to participate in the conduction process. Unlike metals, the resistance of semiconductor material decreases with temperature. As the temperature increases, the thermal energy of the valence electrons increases, allowing more of them to breach the energy gap into the conduction band. When an electron gains enough energy to escape the electrostatic attraction of the atom, it leaves behind a vacancy which may be filled be another electron. The vacancy produced can be thought of as a second carrier of positive charge. It is known as a hole. As electrons flow through the semiconductor, holes flow in the opposite direction. If there are n free electrons in an intrinsic semiconductor, then there must also be n holes. Holes and electrons created in this way are known as intrinsic charge carriers. The carrier concentration or charge density defines the number of charge carriers per unit volume. This relationship can be expressed as $n = p$ where n is the number of electrons and p the number of holes per unit volume. The variation in the energy gap between different semiconductor materials means that the intrinsic carrier concentration at a given temperature also varies.

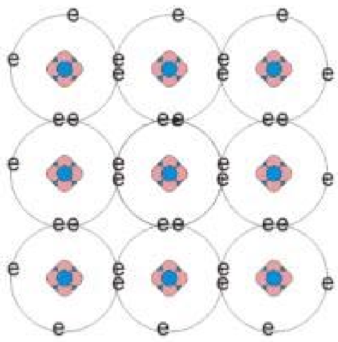

Fig 2-2. This figure shows Intrinsic Semiconductor

— Extrinsic Semiconductors (Doped Semiconductors) —

An extrinsic semiconductor can be formed from an intrinsic semiconductor by added impurity atoms to the crystal in a process known as doping. To take the simplest example, consider Silicon. Since Silicon belongs to group IV of the periodic table, it has four valence electrons. In the crystal form, each atom shares an electron with a neighboring atom. In this state it is an intrinsic semiconductor. B, Al, In, Ga all has three electrons in the valence band. When a small proportion of these atoms, (less than 1 in 10^6), is incorporated into the crystal, the dopant atom has an insufficient number of bonds to share bonds with the surrounding Silicon atoms. One of the Silicon atoms has a vacancy for an electron. It creates a hole that contributes to the conduction process at all temperatures. Dopents that create holes in this manner are known as acceptors. This type of extrinsic semiconductor is known as p-type, and it creates positive charge carriers. Elements that belong to group V of the periodic table such as As, P, Sb have an extra electron in the valence band. When added as a dopant to intrinsic Silicon, the dopant atom contributes an additional electron to the crystal. Dopants that add electrons to the crystal are known as donors and the semiconductor material is said to be n-type.

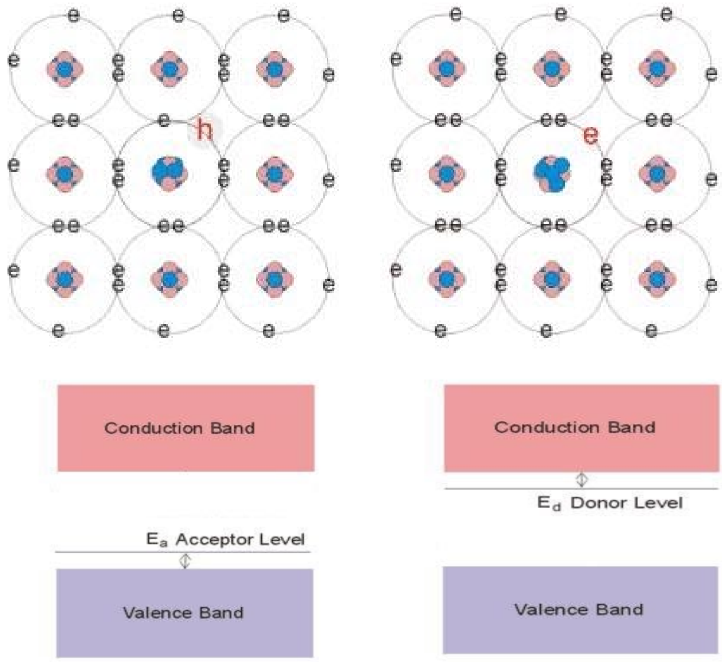

Fig 2-3. This figure shows doped semiconductors. The left is p-type and the right is n-type respectively. Accepter level and donor level are formed in forbidden band. Therefore, electrons are easily excited to the conduction band and contribute to the conduction process.

2-2. p-n Junction Diode

The functioning of all present-day semiconductor detectors depends on the formation of a p-n junction. Such junctions are better known in electronics as rectifying diodes, although that is not how they are used as detectors. Semiconductor diodes can be formed in a number of ways. A simple configuration which we will use for illustration purposes is the p-n junction formed by the juxtaposition of a p-type semiconductor with an n-type material. These junctions, of course, cannot be obtained by simply pressing n- and p-type materials together. Special techniques must be used instead to achieve the intimate contact necessary for junction formation. One method, for example, is to diffuse sufficient p-type impurities into one end of a homogeneous bar of n-type material so as to change that end into a p-type semiconductor.

The formation of a p-n junction creates a special zone about the interface between the two materials. This is illustrated in Fig. 2-4. Because of the difference in the concentration of electrons and holes between the two materials, there is an initial diffusion of holes towards the n-region and a similar diffusion of electrons towards the p-region. As a consequence, the diffusing electrons fill up holes in the p-region while the diffusing holes capture electrons on the n-side. Recalling that the n and p structures are initially neutral, this recombination of electrons and holes also causes a charge build-up to occur on either side of the junction. Since the p-region is injected with extra electrons it thus becomes negative while the n-region becomes positive. This creates an electric field gradient across the junction which eventually halts the diffusion process leaving a region of immobile space charge. The charge density and the corresponding electric field profile are schematically diagrammed in Fig.2-4. Because of the electric field, there is a potential difference across the junction. This is known as the contact potential. The energy band structure is deformed as shown in Fig. 2-4, with the contact potential generally being on the order of 1 V.

The region of changing potential is known as the depletion zone, and has the special property of being devoid of all mobile charge carriers. And, in fact, any electron or hole created or entering into this zone will be swept out by the electric field. This characteristic of the depletion zone is particularly attractive for radiation detection. Ionizing radiation entering this zone will liberate electron-hole pairs which are then swept out by the electric field. If electrical contacts are placed on either end of the junction device, a current signal proportional to the ionization will then be detected.

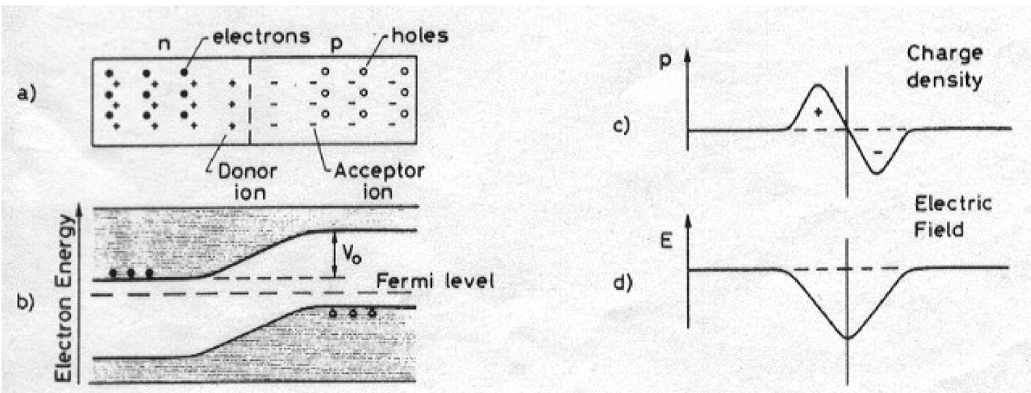

Fig 2-4. (a)Schematic diagram of an p-n junction, (b)diagram of electron energy levels showing creation of a contact potential V_0, (c)charge density, (d)electric field intensity.

While the p-n junction described above will work as a detector, it doesn't present the best operating characteristics. In general, the intrinsic electric field will not be intense enough to provide efficient charge collection and the thickness of the depletion zone will be sufficient for stopping only the lowest energy particles. This small thickness also presents a large capacitance to the electronics and increases noise in the signal output. Better results can be obtained by applying a reverse-bias voltage to the junction, i.e., a negative voltage to the p-side, as shown in Fig. 2-5. This voltage will have the effect of attracting the holes in the p-region away from the junction and towards the p contact and similarly for the electrons in the n-region. The net effect is to enlarge the depletion zone and thus the sensitive volume for radiation detection – the higher the external voltage, the wider the depletion zone. Moreover, the higher external voltage will also provide a more efficient charge collection. The maximum voltage which can applied, however, is limited by the resistance of the semiconductor. At some point, the junction will breakdown and begins conducting. [3]

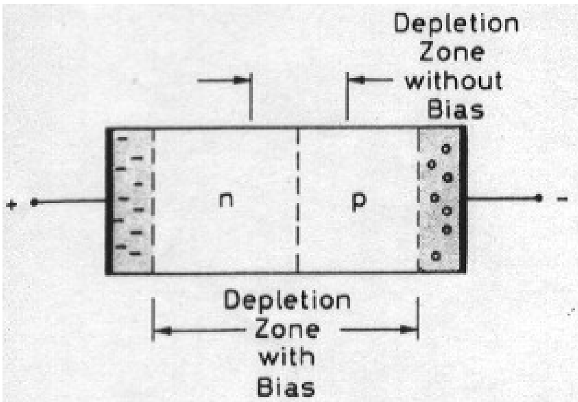

Fig 2-5.   Reversed-bias Junction

2-3. Principle of Semiconductor Detectors

When a reverse bias voltage is applied to a p-n junction diode, a depletion zone spreads from the p-n junction. If the impurity concentration of p-side is enough higher than that of n-side, the depletion zone extends into the n-side with the increase of a reverse bias voltage. When the n-type semiconductor is fully depleted, we call its reverse bias voltage “full depletion voltage”. We usually use this full depletion zone in the n-side as a sensitive region. If an ionizing radiation particle comes into the full depletion zone, the incident particle creates many electron-hole pairs by the coulomb interaction. They are respectively attracted to each electrode in the opposite sides by an electric field formed by the reverse bias voltage, and these are detected as a signal. This is the fundamental principle of a semiconductor detector. Figure 2-6 shows the basic outline of a semiconductor detector. [4]

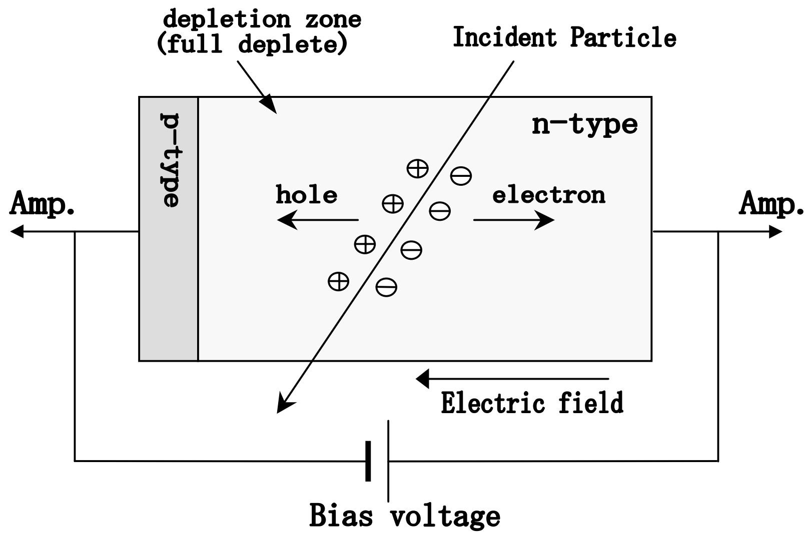

Fig 2-6. Operating principle of the semiconductor detector

2-4. AC-coupled Silicon Strip Sensor

Silicon strip sensor is the device of a position measuring semiconductor detector and the concept of position detection is analogous to gas detector. Fig 2-7 shows the cross section of an AC-coupled Silicon strip sensor. This sensor has high doped silicon strips on an n-type silicon wafer which is called n-bulk and also has n^+ plane on the opposite side of the wafer. The strip is p-type silicon and called p^+-strip. Each strip functions as an independent position sensor. The p-n junctions are formed between the p^+-strips and the n-bulk. There is also an Al-electrode on a strip across a SiO_2 that is an insulator. The strip and the Al-electrode function as a capacitor. This structure is an AC-coupling. The surface of the sensor is covered with the SiO_2 which is called passivation. If an Al-electrode is directly connected with a strip, the leakage current is detected as a background noise. Because this leakage current increases with the radiation damage, at the end, it breaks a preamplifier to read out signal. Owing to the function of the capacitance between a p^+-strip and an Al-electrode, however, we can read out the change of the potential in a strip as a signal from an Al-electrode.

By applying a reverse bias voltage between p^+-strips and n^+ plane, a depletion zone extends from p-n junction toward the n-bulk. If an ionizing particle comes into this zone after fully depleted, the valence electrons of silicon atoms are excited by the energy of this particle and electron-hole pairs are created along the particle track. The holes are attracted to the nearest p^+-strips and the electrons are attracted to the n^+ plane, respectively, by an electric field caused by a reverse bias voltage. Thus, by the function of the capacitor between the Al-electrode and the p^+-strip, the opposite charges of which the absolute quantities are equal to those of the attracted charges in the strip are induced to the Al-electrode. As a consequence, the positive charges flow into the preamplifier and are read out as a signal. Hence, we can find the incident position of the particles by identifying the strip which has a signal.

However, it must be careful that silicon strip sensor must always be operated at low temperature. For silicon strip sensors, increasing temperature result in higher leakage currents and greater noise. The leakage current is sensitive to the temperature showing an increase by a factor two with an increase in temperature of 7.5℃. And also the high leakage current will cause irreversible damage to the crystal.

But the silicon strip sensor has advantages as follows in comparison with the gas detector. Silicon has a good efficiency because these high-density materials have a heavy energy loss. Besides, we can reduce the volume of a sensor compared with a gas chamber because of it’s high-density. And an electron and hole have a large mobility. Consequently, its collection time is very short. Therefore, the onset time of a pulse is very fast on silicon strip sensors.

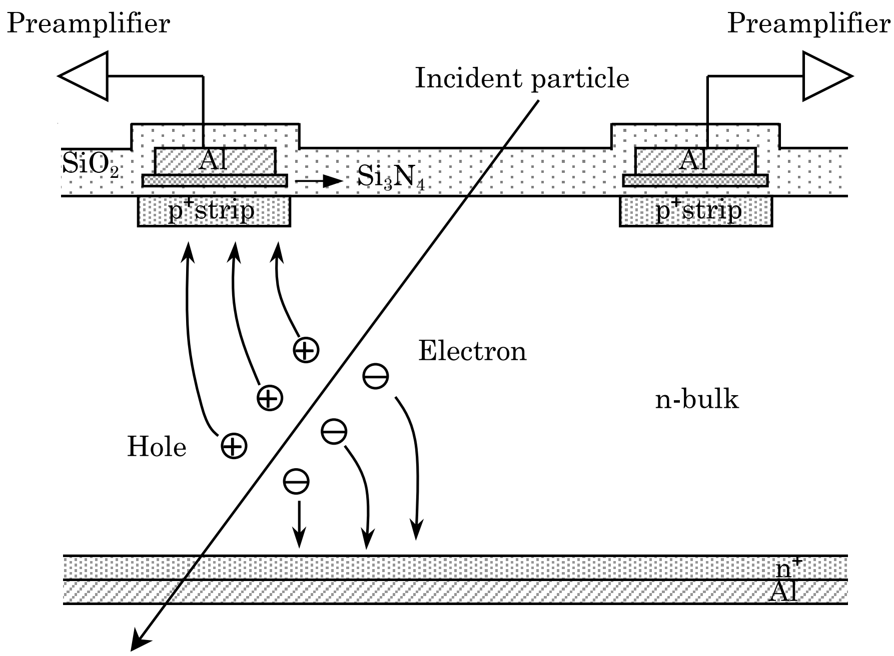

Fig 2-7. The cross section of an AC-coupled Silicon strip sensor

2-5. Radiation Damage

When an AC-coupled silicon strip sensor for GLAST is used in the space, the sensor suffers radiation damages by the cosmic-ray and its performance becomes lowers. There are two kinds of the radiation damages. One is a "surface damage" and the other a "bulk damage". The surface damage occurs in the surface of the sensors literally. This causes the breakdown of the leakage current and the noise amplification at the lower bias voltage. The bulk damage occurs in the n-bulk and the leakage current get higher due to this damage. These two damages occur simultaneously. In the worst case, the breakdown of leakage current and the noise amplification begin before the sensor depletes fully and the sensor does not work as a detector. The details of two kinds of the radiation damage are as follows. [5]

- Bulk damage (displacement damage)-

When the high-energy particles enter into the n-bulk, the lattice atoms are displaced from original lattice position by interaction with incident particles and defects or interstitial atoms appear. This is called displacement damage. The defects create energy levels in the forbidden band. As a consequence, it causes an increase of the leakage current.

Leakage current I_{leak} is expressed as the sum of initial leakage current I_0 and a term which is proportional to the absorption dose.

$$I_{leak} = I_0 + \alpha \cdot \Phi$$

Here, I_0 is initial leakage current, Φ is radiation fluence and α is leakage current constant, which is determined by irradiation particle and its energy. The value of α is generally defined at $t = \infty$, because annealing after irradiation is a function of time.

It is thought that the increase of leakage current by radiation damage is due to radiation-induced energy levels in the forbidden band which works as generation center. Of course, the levels near the center of forbidden band contribute greatly. The damage is defects or interstitial atoms, and they can move freely. If each satisfies, they disappeared. Also, the defects concentrate and make a cluster. The move speed of a defect is a function of temperature, and the probability that the defects encounter each other is expressed as follows:

$$p = A\exp\left(-\frac{E}{kT}\right)$$

Here, E is an activation energy, A is a constant and k is the Boltzmann constant. This formula shows that the annealing is a function of a temperature.

- Surface damage -

The surface of the sensor is covered with an insulator SiO_2. If ionizing particle comes into this layer, electron-hole pairs and defects are created there. The mobility of an electron is high at room temperature, and thus these electrons scatter and disappear regardless of existence of an electric field. On the other hand, the mobility of a hole is smaller than that of an electron, and holes are easily trapped by defects in the SiO_2 layer. It is known that the holes are liable to be trapped especially at the interface between SiO_2 layer and n-bulk. These trapped holes result in the accumulation of positive charge in the SiO_2 layer. This positive charge makes mainly three problems on sensor as shown in the following.

(1) It makes a high electric field at the strip edge, which causes a microdischarge even at low bias voltage. As a consequence, the noise amplification increases steeply.
(2) This positive charge makes energy levels in the forbidden band. Consequently, it increases the leakage current.
(3) This positive charge trapped inside the SiO_2 layer attracts electrons along the surface of n-bulk and the electrons make a thin conductive layer (an electron accumulation layer) underneath of the SiO_2. The conductive layer spoils the strip to strip isolation.

The surface damage recovers with time. It is thought that the mechanism of this annealing is explained in such a way that holes recombine with electrons in the n-bulk through the tunneling effect. The time scale of annealing is a few days.

Chapter 3
Silicon Strip Sensors for GLAST

3-1. Requirements and Specifications

The specifications for parameters of a silicon strip sensor are listed in table3-1.

(1) Full depletion voltage

When a reverse bias voltage is applied to a silicon sensor, a depletion zone spreads from the p-n junction. Because the impurity concentration of p-side is enough higher than that of n-bulk, the depletion zone expands into the n-bulk with the increase of a reverse bias voltage. When the n-bulk is fully depleted, we call this reverse bias voltage "full depletion voltage".

The operation of sensors under the low bias voltage is desirable for a space mission where limited power and the potential for arcing are a problem, thus the full depletion voltage must be as low as possible. The specification of the full depletion voltage is <120V. The full depletion voltage depends on the resistivity of wafer and 120V is reasonably low value under the current wafer situation.

In order to find the full depletion voltage of a silicon sensor, it is needed to measure the capacitance of the n-bulk which is called "body capacitance (C_{Body})". The inverse square of the capacitance increases with the increase of a reverse bias voltage and gets almost constant at some voltage. This means that the sensor is fully depleted.

We defined the full depletion voltage as follows: we fitted a linear in value of $1/C^2$ before and after the point where $1/C^2$ gets constant respectively and defined a full depletion voltage with a point of interaction of two lines. This is shown in Fig3-1.

(2) Leakage current

An ideal p-n junction diode is non-conducting when it is applied the reverse bias voltage and also a semiconductor is non-conducting at 0K except for Ge. But it is impossible to fulfill this condition in fact. In general, a small fluctuating current flows through the semiconductor detector when reverse bias voltage is applied to it. This current is called "leakage current". The leakage current is sensitive to the temperature showing an increase by a factor two with an increase in temperature of 7.5℃ [6].

The leakage current appears as noise at the sensor output and sets a limit on the smallest signal pulse height which can be observed. The leakage current is very important parameter because it effects noise and power consumption. The low-leakage current sensor is desirable. The equivalent noise charge (ENC) of the shot noise by the leakage current is expressed as follows:

$ENC = 150\sqrt{I \cdot dt}$ electrons (3.1)

Here, I is the leakage current in nA and dt is the peaking time in μsec. The peaking time of the preamplifier for the GLAST is 2μs.

The leakage current of the silicon strip sensor is a direct evidence of the fabrication quality. Almost all kind of imperfection contributes leakage current, either generated at the interface underneath the surface oxide (surface leakage current) or in the bulk. Therefore, a leakage current measurement is the most straightforward and simple diagnostic tool for entire sensors and individual channels. The total leakage current reflects the junction quality and the surface quality of the junction side, because only on the junction side, the energy levels of surface defects in the forbidden band contribute to the generation of the leakage current [7]. The leakage current of silicon strip sensors for GLAST already satisfies the physical requirements and the specification was set to reasonably achievable value.

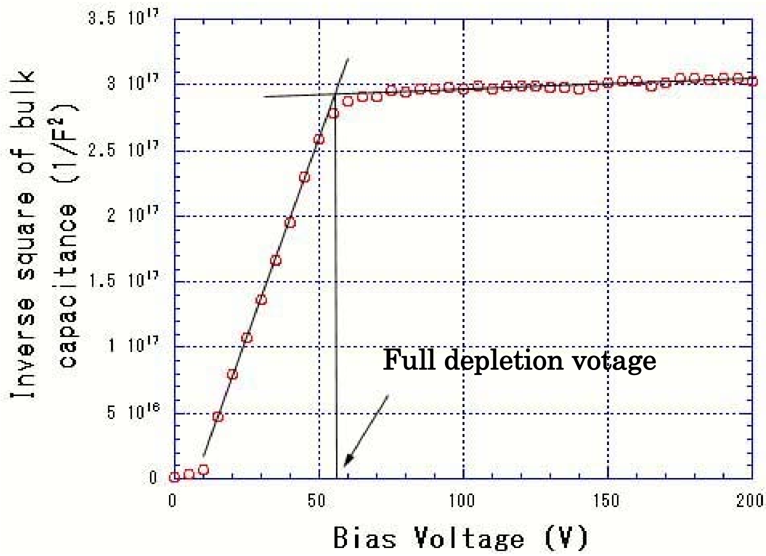

Fig 3-1. Definition of the full depletion voltage

(3) Coupling capacitance

The coupling capacitance is defined as that between p^+ strip and Al electrode. If the coupling capacitance is small, the signal in p^+ strip is hard to transmit to Al electrode.

In other words, the signal is lost partially. Thus the coupling capacitance is desired as large as possible. The coupling capacitance of silicon strip sensors for GLAST already satisfies the physical requirements and the specification was set to reasonably achievable value. The coupling capacitance (C_{CP}) is charted in Fig3-3.

(4) Interstrip capacitance

Interstrip capacitance is defined as that between one Al electrode and its neighbors. In the silicon strip sensor, the signal is read out from Al strip through the AC coupling capacitor. Here, if the interstrip capacitance is too large, the charges induced in the Al strip are distributed over plural Al strips. As a consequence, it results in the increase of the noise. Then the low interstrip capacitance is desired. The interstrip capacitance of silicon strip sensors for GLAST already satisfies the physical requirements and the specification was set to reasonably achievable value. The interstrip capacitance (C_{Int}) is charted in Fig3-3.

(5) Bias resistor resistance

In the bias resister resistance, there is an upper limit and a lower limit. The time constant (τ =CR, ; Here, C is the sum of C'_{Int}(see Fig3-3) and the capacitance between a p^+ strip and the back plane of the silicon strip sensor) has to be much larger than the readout time. The bias voltage is applied to all p^+ strips through the bias resister, which keeps the independence between strips. If the bias resister resistance is too high, the voltage applied to the strips becomes reduced due to voltage drop (V=IR). On the contrary, if the bias resister resistance is too small, the strip by strip independence is lost. The bias resistor is charted in Fig3-2.

(6) Faulted strip rate

The faulted strip is defined as follows:

・Coupling capacitor(p^+ strip - Al strip) shorts
・Bias resister is open
・Al strip is open
・Bad isolation between neighboring p^+ strips
・Bad isolation between neighboring Al strips

The faulted strips affect the reconstruction of the particle track. The requirement for the faulted strip rate is decided from the results of the simulation.

(7) Interstrip resistance

The interstrip resistance is defined as that between one p^+ strip and its neighbors. It is important in characterizations of silicon strip sensors because if the interstrip resistance is too small, the strip by strip independence is lost and consequently results in charge spreading and the reduction of sensor resolution [8]. And thus, it is desired as large as possible. The specification of interstrip resistance is >1GΩ. The interstrip resistance (R_{Int}) is charted in Fig3-2.

parameters	Before irradiation	After gamma-ray irradiation with a dose of 10krad
Full depletion voltage	<120V	
Leakage current density at 25℃	<3nA/cm^2 (average) <10nA/cm^2 (maximum)	<120nA/cm^2
Coupling capacitance	>500pF	
Interstrip capacitance	<1.5pF/cm	<1.6pF/cm
Bias resister resistance	>20MΩ , <80MΩ	
Faulted strip rate(averaged over every 100sensors)	<0.2%	
Maximum number of faulted strips/sensor	<3strips (0.8%)	
Interstrip resistance	>1GΩ	>1GΩ

Table 3-1. The specifications of the parameters of silicon strip sensor.

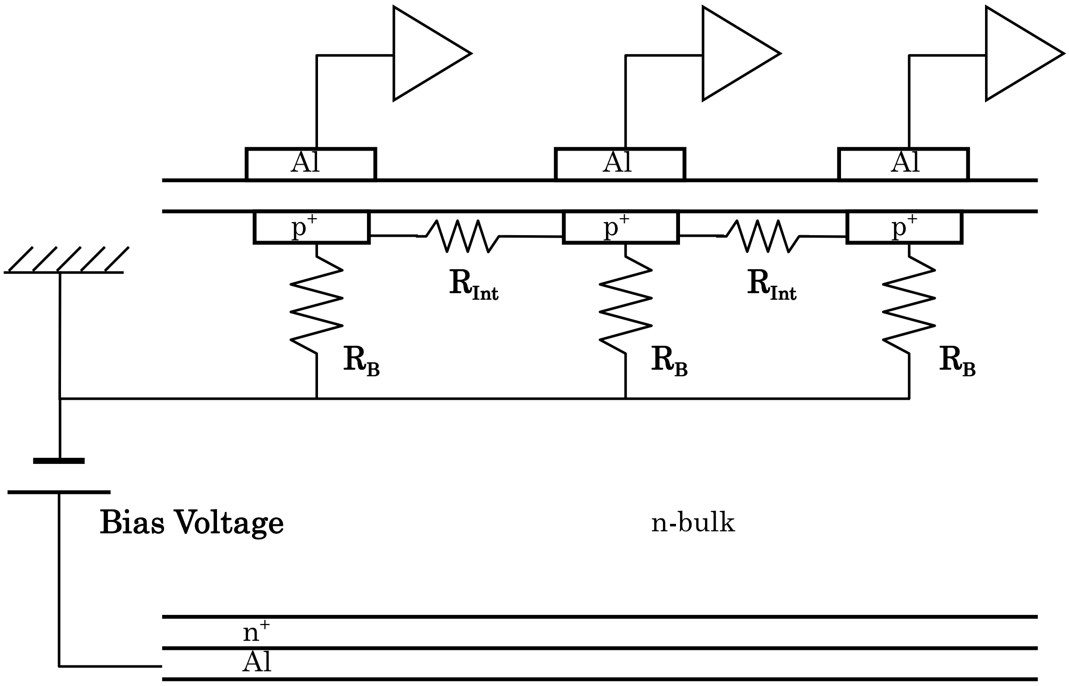

Fig 3-2. The circuit of the silicon strip sensor.

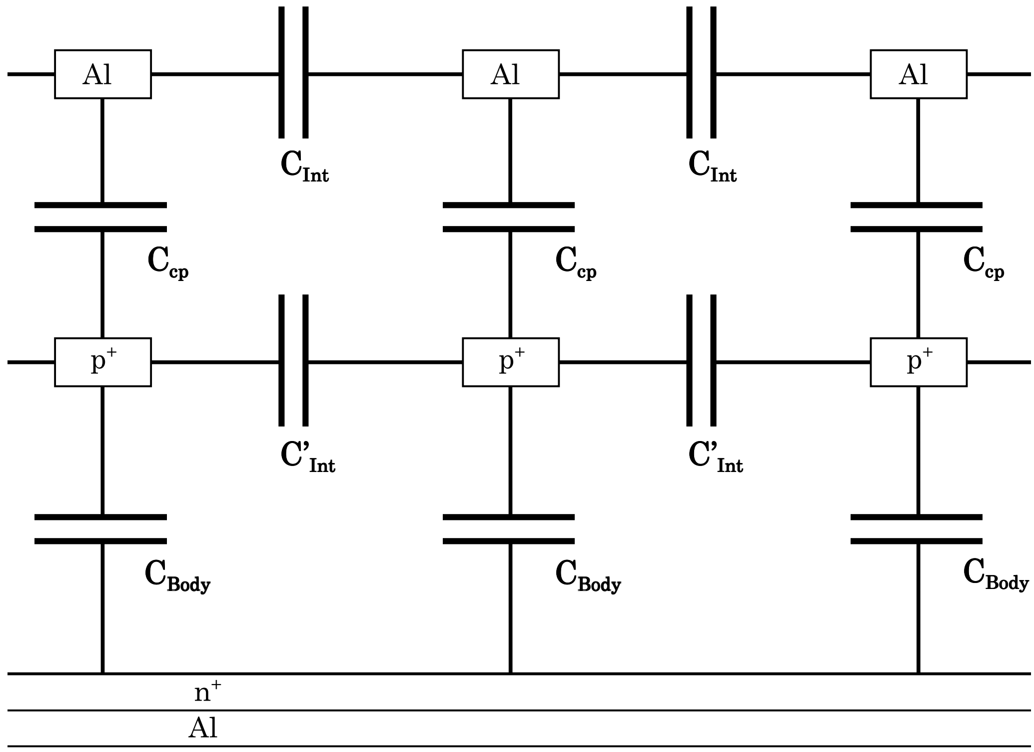

Fig 3-3. The model circuit for the capacitance of the silicon strip sensor.

3-2. Structure

The surface structure and the cross section of a silicon strip sensor (SSD) are shown in Fig3-5 and 3-6, respectively. The SSD for GLAST is fabricated on the 6-inch high-resistivity (5kΩ-cm) wafer which is the largest area for this high-resistivity wafer. The wafer is n-type and its surface crystal orientation is (100). The full size SSD has 384 high doped silicon strips with 228 μm pitch on one side of the n-bulk. The test sensor which contains 8 strips with the same strip parameter is also fabricated at the edge of the wafer. The thickness of the sensor is 410 μm and the width of the p^+ strip and Al strip is 56 μm and 64 μm respectively.

The surface of the sensor is covered with SiO_2 passivation layer except for the pads and a part of the bias ring, in order to insulate and protect the surface structure.

A p^+ strip and an Al strip make an AC-coupling structure through the dielectric and the signal is read out from the Al strip. This structure prevents saturating the preamplifier by the leakage current increased by the radiation damage when the signal is read out. Here, the dielectric is combination of SiO_2+Si_3N_4. If the dielectric is only SiO_2, the pinholes will appear on it. In order to prevent this situation, the double film structure is adopted.

The outer size of the full size sensor and the test sensor is 8.9500×8.9500 cm and 8.9500×0.3772 cm, respectively. The picture of these sensors on the 6-inch wafer is shown in Fig3-4.

-DC Pad-

This is the electrode which is electrically connected to the p^+ strip.

-AC Pad-

This is the electrode which is electrically connected to the Al strip.

-Bias Resister and Bias ring-

The bias resister is made with polysilicon, since it was proved to be radiation-hard. A wide range of resistance value can be achieved because the polysilicon resistor is installed over a SiO_2 insulator plane, which allows us to install long resistor without any loss of sensitive area. A typical resistivity of radiation-hard polysilicon resistor is 1-4MΩ/mm for 5 μm wide line. Lower resistivity resistors made with higher doped polysilicon are found to be more uniform in resistivity and more stable under high radiation. All p^+ strips are connected to the bias ring through the bias resistor, which is grounded in use. [9]

-Guard ring-

The silicon strip sensor is cut out from the wafer with diamond saw. Thus, there are a lot of cracks in the crystal at the edge of the sensor. These cause the breakdown and the increase of the leakage current of the sensor. The guard ring plays a role as separator between this cracked area at the edge of the sensor and the sensitive area.

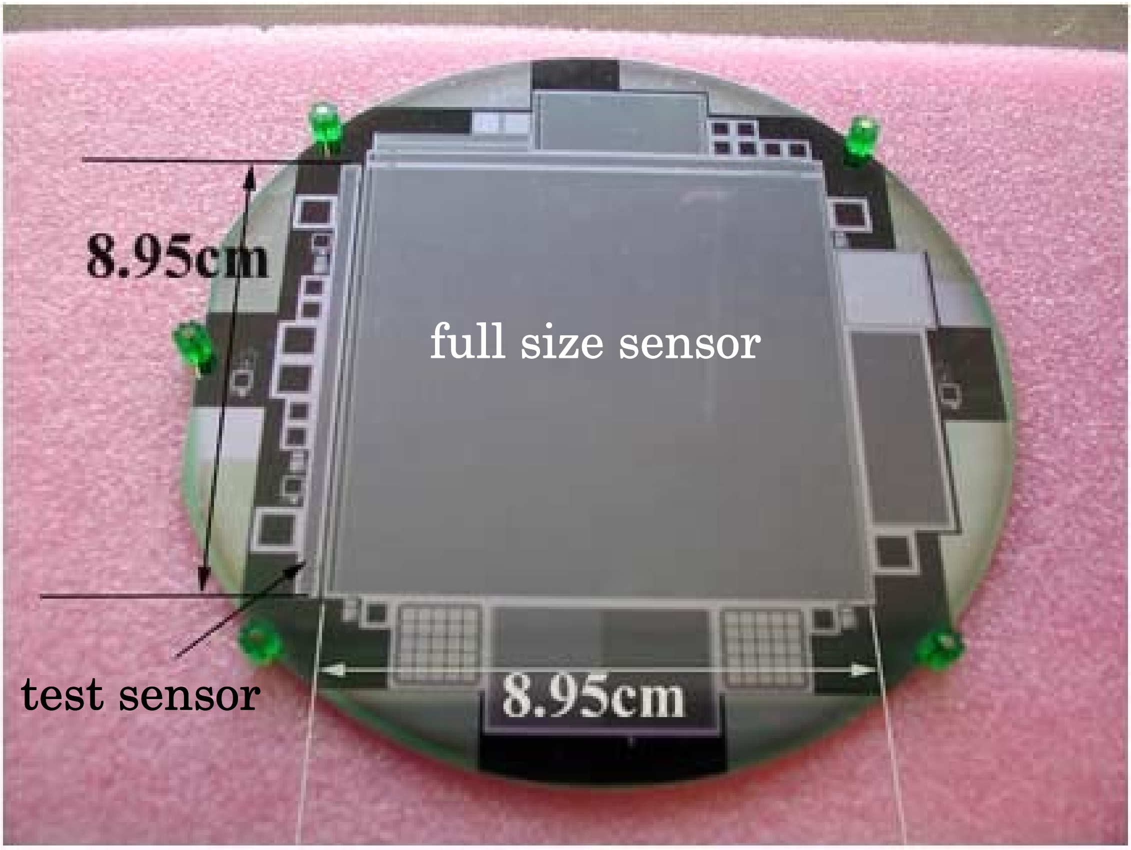

Fig 3-4. The full size and test sensor on 6-inch wafer. The biggest square part at the center is the full size sensor for GLAST FM sensor. The portion of a long and slender rectangle is a test sensor to the left of the full size sensor.

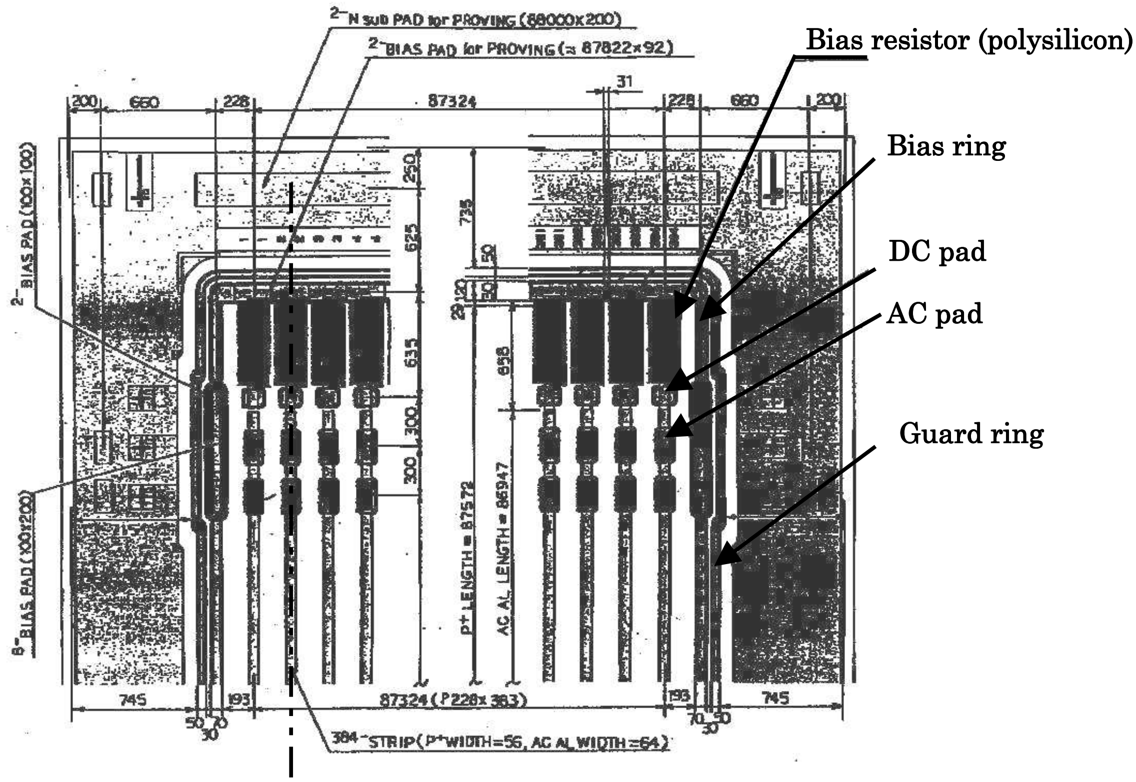

Fig 3-5. The surface structure of the silicon strip sensor for GLAST.

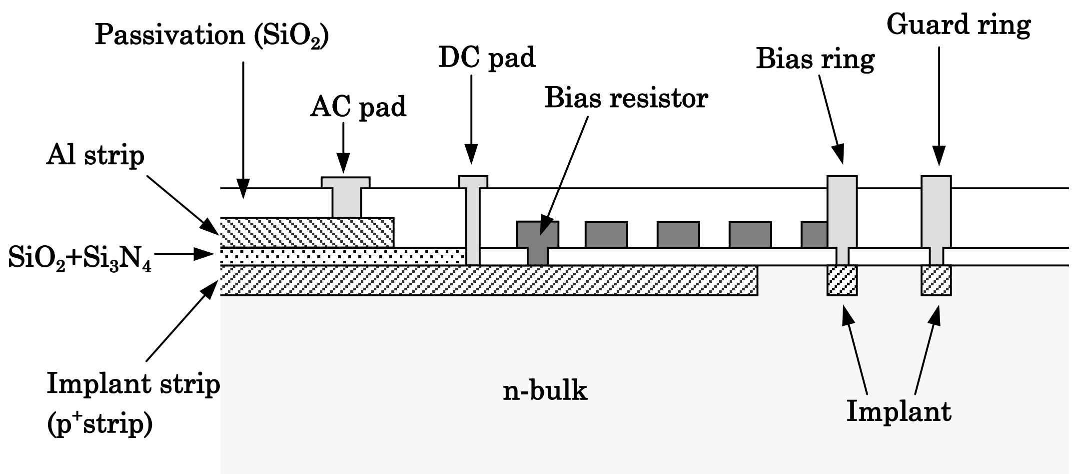

Fig 3-6. The cross section at the dashed line in Fig3-5.

3-3. Production

The total number of silicon strip sensors for GLAST LAT is about 10,000. These silicon strip sensors have been manufactured by Hamamatsu Photonics (HPK), which is the world's premier supplier of SSD with large production and testing capacity, and a specialist for radiation tolerant SSD. The mass production of sensors has began since Feb. 2001 and over 1,000 SSD have been produced and 622 have been investigated in detail by now (Jan. 2002). Hereafter, the remainder is to be produced in 500 monthly outputs, that is, 10,000 in 2 years.

The construction of the trays, on which the silicon strip sensors are attached, started at the beginning of 2002. The construction of the LAT will start in Dec. 2002 at SLAC and be finished in Apr. 2004. Then, the LAT will be attached on the satellite in Apr. 2005 and GLAST will be launched by NASA with the delta II rocket in Mar. 2006.

3-4. Purpose of This Thesis

We have investigated the performance of pre-produced silicon strip sensors for GLAST before mass production. The leakage current, full depletion voltage, coupling capacitance, interstrip capacitance, bias resistor resistance, faulted strip rate and the effect of radiation damage were investigated and we confirmed that those results satisfied the specification for GLAST mission. This study is reported in section 4-2.

The mass production of FM silicon strip sensors has began in Feb. 2001. We investigated the performance of these sensors for the verification. We also investigated the effects of radiation damage of sensors as means to monitor the fabrication process. This is reported in section 4-3.

The leakage current of these sensors is very low and its value is comparable to a low-leakage current photodiode. This kind of low-leakage current sensor has not existed before. We investigated the radiation damage of low-leakage current sensors because there might be unknown phenomena. First of all, we measured the relation between the gamma-ray dose and increase of the leakage current. This is reported in section 5-1. Then we investigated the effect of the radiation damage for applying the bias voltage to the sensor. This is reported in section 5-2.

Chapter 4
Verifications of Flight-Model Silicon Strip Sensors

4-1. Flow of Verifications

The silicon strip sensors for GLAST have been manufactured by Hamamatsu Photonics (HPK) and verificated at Hiroshima, SLAC/UCSC and INFN-Pisa. Until the geometry of the present silicon sensors is established, many researches have been made and some modifications have been done. Table4-1 summarizes the development of the silicon strip sensor for GLAST.

In 1996, the silicon strip sensor on the 4-inch high-resistivity wafer was fabricated. The size of this sensor was 6×6cm and punch through resistor was adopted as a bias resistor. In 1997, the size of the sensor was changed to 6.4×6.4cm which is the maximum size fabricable for the 4-inch wafer and the bias resistor has changed to the polysilicon resister since this year. In 1998, high-resistivity 6-inch wafer technology was developed. Then, the test silicon strip sensor was fabricated on the 6-inch wafer in 1998. These sensors were tested and satisfied the requirements. Consequently the silicon strip sensors on the 6-inch wafer were fabricated in 1999. The size of these sensors was 9.5×9.5cm which is the maximum size fabricable for the 6-inch wafer. In addition to these changes, the surface crystal orientation of the sensor has changed to (100) for its good availability, while the (111) sensor had been used [10]. The (100) sensors were tested in Hiroshima and we confirmed that the performance of (100) is equal to (111) [11]. And thus it was decided that the surface orientation of (100) is adopted in the silicon strip sensor for GLAST. In Dec. 2000, the first pre-mass produced 35 sensors were manufactured. The size of the silicon strip sensor was changed to 8.95×8.95cm, because the size of 9.5×9.5cm was somewhat too large when having considered the size of the rocket. The performance of these sensors was verified in Hiroshima and satisfied the specification for full depletion voltage, leakage current, coupling capacitance, interstrip capacitance, bias resister resistance and faulted strip rate. The heavy ion and gamma-ray tolerance of these sensors were enough for GLAST mission. As a consequence, it could shift to mass production with the same fabrication process.

	1996	1997	1998	1999	2000
Wafer Size	4-inch	4-inch	6-inch	6-inch	6-inch
Sensor Size [cm×cm]	6×6	6.4×6.4	6.4×10.7	9.5×9.5	8.95×8.95
Pitch	236 μm	194 μm	194 μm	208 μm	228 μm
Implant Width	57 μm	50 μm	50 μm	52 μm	56 μm
Thickness	500 μm	400 μm	400 μm	400 μm	400 μm
Biasing	Punch Through	Polysilicon	Polysilicon	Polysilicon	Polysilicon
Surface orientation	(111)	(111)	(111)	(100)	(100)

Table 4-1. The development of the silicon strip sensors.

4-2. Verifications of Pre-Mass Production

We have investigated the performance of pre-produced 35 silicon strip sensors (SSD) for GLAST before mass production in order to confirm that those sensors satisfy the specification for GLAST mission.

4-2-1. Measurement Items

The following items were measured for all 35 sensors by HPK and 5 of them were also measured in Hiroshima in this verification.

(1) Full Depletion Voltage
(2) Leakage Current
(3) Coupling Capacitance
(4) Interstrip Capacitance
(5) Bias Resistor Resistance
(6) Faulted Strip Rate

4-2-2. Set up for Measurements

(1) Full depletion voltage

Fig4-1 shows how the body capacitance was measured. In order to find the depletion voltage, the bias voltage dependence of the bulk capacitance was measured. The 0～200V reverse bias voltage was applied to the n^+ and the bias ring was grounded. Here, the Al electrodes were electrically floating. For this measurement we use HP4284 LCR meter. Here, the frequency of the LCR meter was set at 100Hz. The probe which is connected to the high terminal was put down on the n^+(back plane), while the probe of the low terminal is put down on the bias ring.

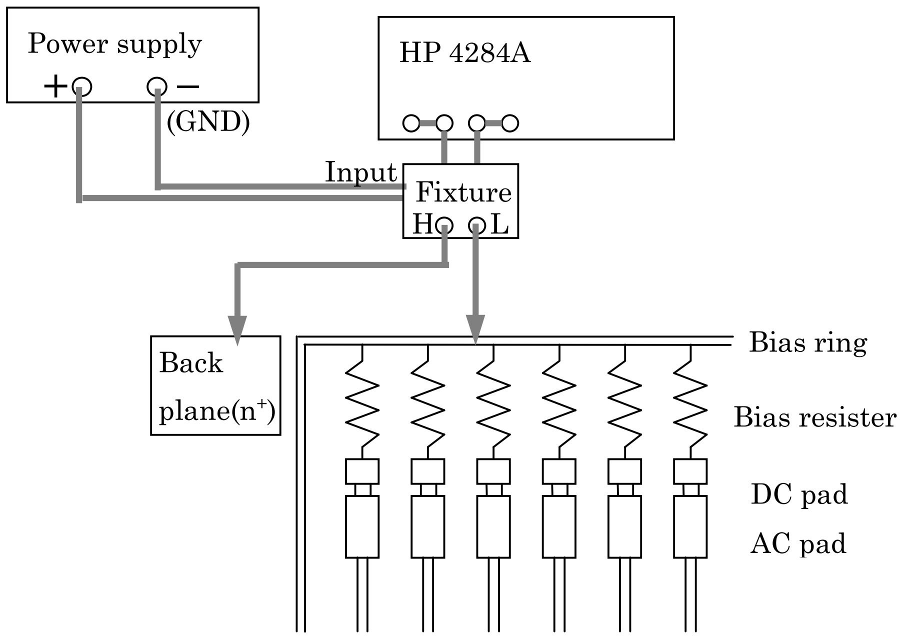

Fig 4-1.　The set-up for the measurement of body capacitance

(2) Leakage current

Fig 4-2 shows how the leakage current was measured. In order to examine the bias voltage dependence of the leakage current, the 0～200V reverse bias voltage was applied to the n^+ and the bias ring was grounded. Here, the Al electrodes were electrically floating. The total leakage current was read out from the bias ring by putting down the probe on it. The temperature was kept constant at 20℃ during the measurement.

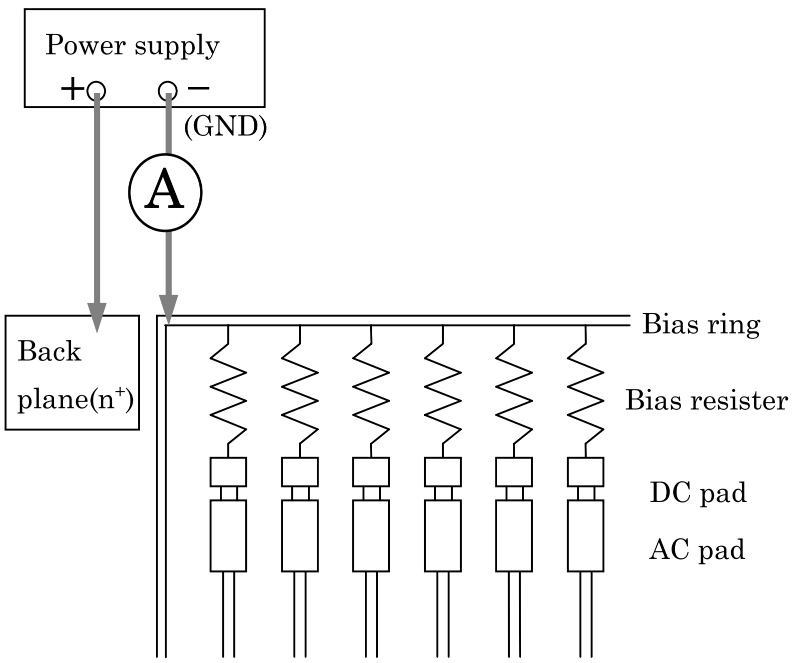

Fig 4-2. The set-up for the measurement of leakage current

(3) Coupling Capacitance

Fig4-3 shows how the coupling capacitance was measured. In order to measure the coupling capacitance of each sensor, the 150V reverse bias voltage was applied to the n^+ and the bias ring was grounded. The coupling capacitance mainly corresponds to the thickness of SiO_2, and also it is hard to think that the thickness is so much irregular throughout the surface of the sensor. Therefore, we selected only 1,2,3,192,382,383, 384th strips to examine the absolute value and the gradient of the coupling capacitance throughout the surface of the sensor. For this measurement we use HP4284 LCR meter and its frequency was set at 100Hz. The probe which is connected to the high terminal was put down on the AC pad, while the probe of the low terminal is put down on the DC pad.

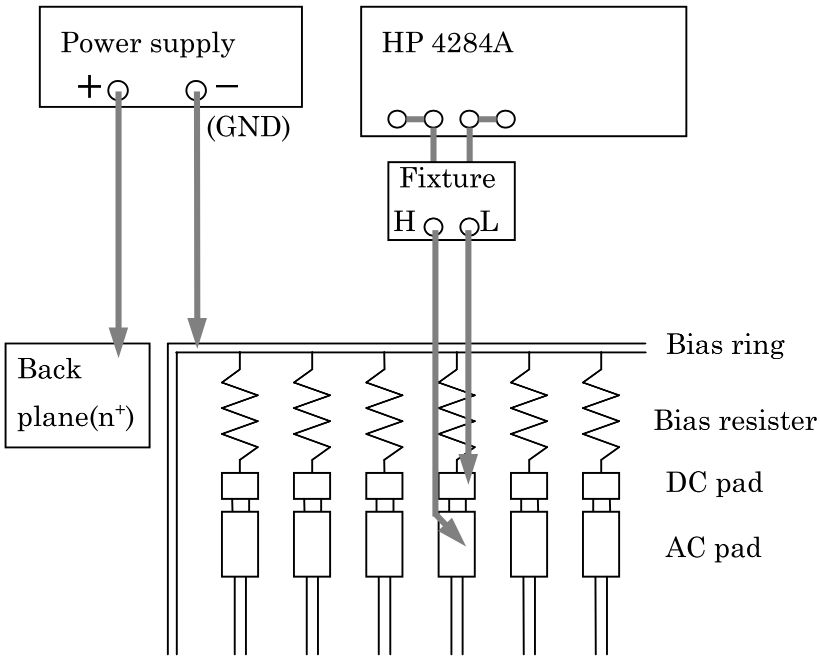

Fig 4-3.　The set-up for the measurement of coupling capacitance

(4) Interstrip Capacitance

Fig4-4 shows how the interstrip capacitance was measured. In order to measure the interstrip capacitance of each sensor, the 150V reverse bias voltage was applied to the n^+ and the bias ring was grounded. For this measurement we use HP4284 LCR meter and its frequency was set at 1MHz. The measured strips were only 2,3,192,382,383th strips. Here, only the capacitance between one AC pad and its neighbors was measured because the capacitance between one strip and its neighbor strips is dominant.

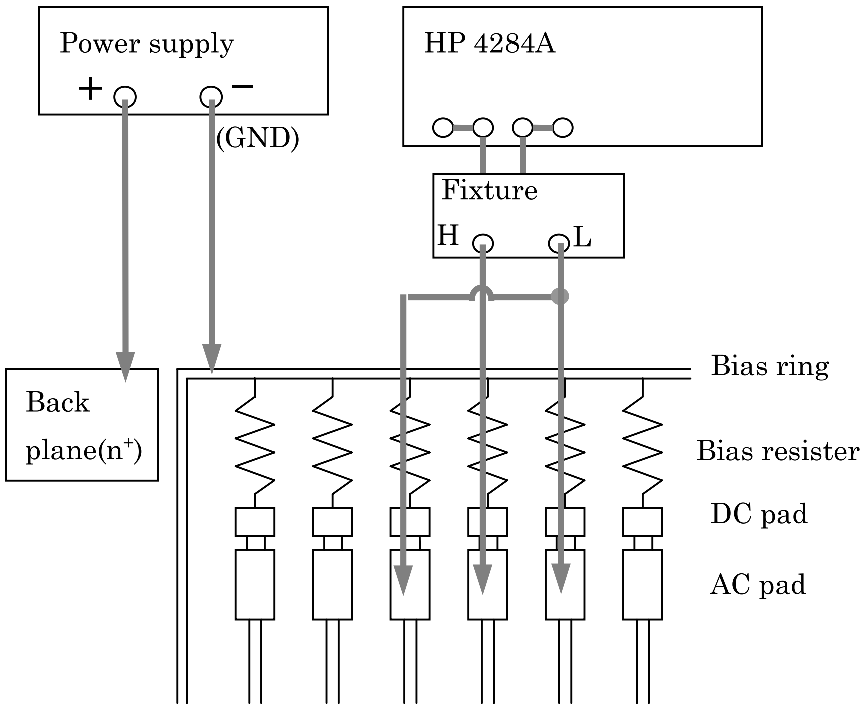

Fig 4-4. The set-up for the measurement of interstrip capacitance

(5) Bias Resister Resistance

Fig 4-5 shows the set-up for the measurement of the bias resister resistance. In order to measure the bias resister resistance of each sensor, the 150V reverse bias voltage was applied to the n^+ and the bias ring is grounded. Here, the Al electrodes were electrically floating. Then, the 3V were applied to the DC-pad and the current which flows in the current meter was measured. The measured strips were only 1,2,3,192,382,383,384th strips. The bias resister resistance was calculated from the current with Ohm's law. But in this method, the current which flows in the current meter contains the leakage current of the sensor, and thus it has to be subtracted from the current. In other words, Resistance = 3V / (current at 3V – current at 0V)

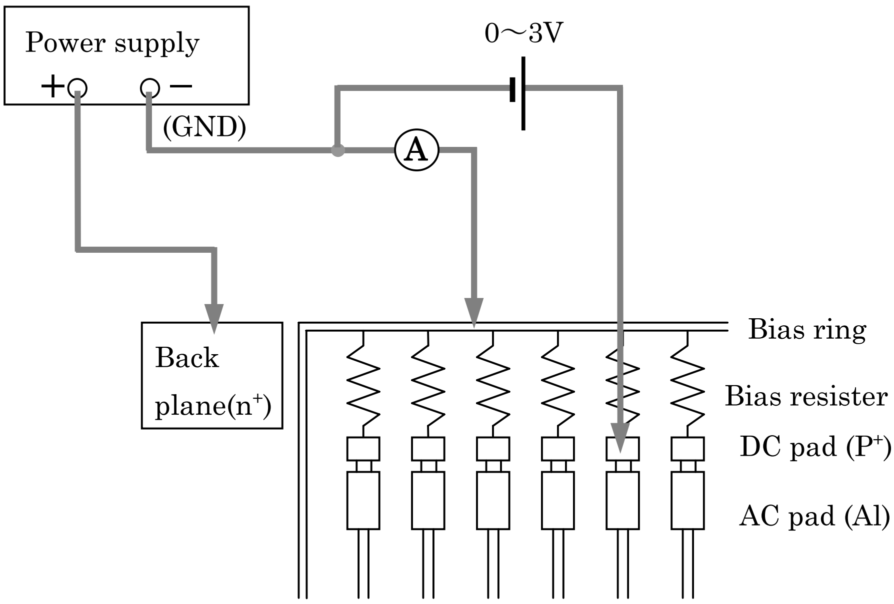

Fig 4-5. The set-up for the measurement of bias resister resistance

4-2-3. Results

(1) Full depletion voltage

Fig4-6 shows the body capacitance of 5 sensors and also $1/C^2$ is plotted in Fig4-7 so as to determine the full depletion voltage easily. As one can see, the full depletion voltage of every sensor is about 60V and the specification of <120V is satisfied enough. This full depletion voltage is relatively low for 410 μ m thick sensor and is due to the use of high resistivity wafer. The operation of sensors under the low bias voltage is desirable for a space mission because the electric power is limited and moreover, vacuum discharge may occur if the operation voltage is high. Table4-1 summaries the full depletion voltage of each sensor.

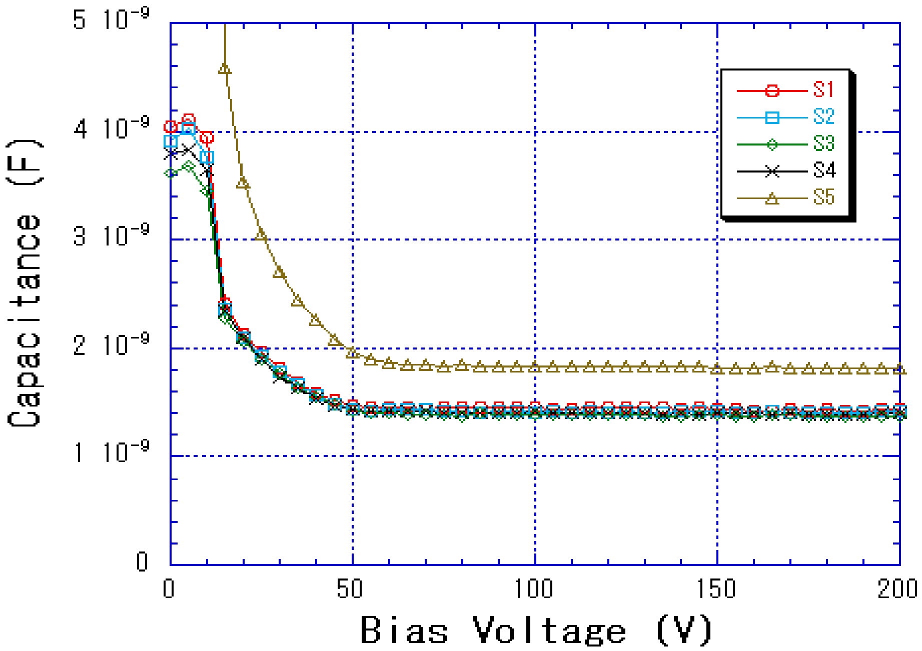

Fig 4-6. The bias voltage dependence of the bulk capacitance. As one can see, the value of the sensor S5 is different from others. This is because S5 is mounted on the PC board for the gamma-ray irradiation test, which is reported in 4-2-4.

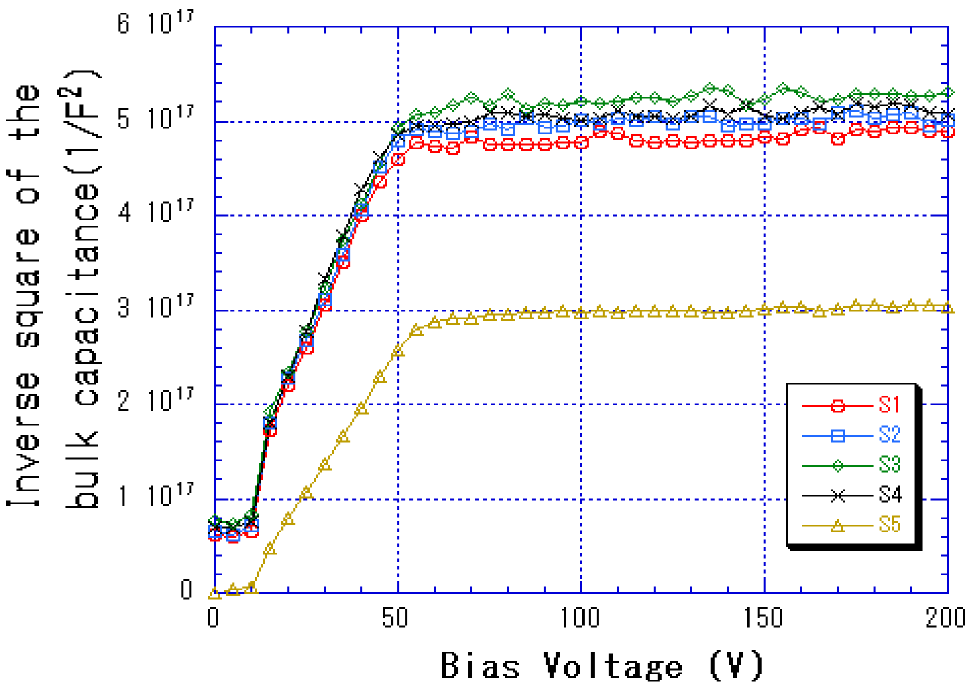

Fig 4-7. The bias voltage dependence of the bulk capacitance. Plotted is the inverse square of the bulk capacitance in order to allow an easier determination of the full depletion voltage.

Sample	S1	S2	S3	S4	S5	spec
Full depletion Voltage (V)	55	55	60	55	60	<120

Table 4-1. Full depletion voltage of 5 sensors.

Fig4-8 shows the distribution of full depletion voltage for all sensors measured by HPK and S1～5 are included in it. As one can see, all sensors fully satisfy the specification of <120V.

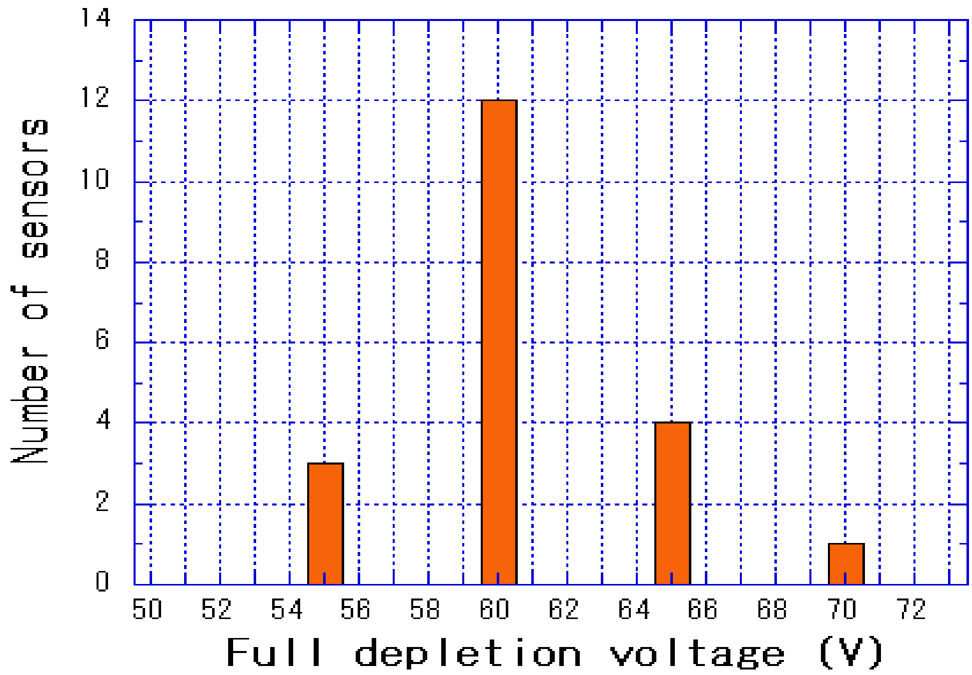

Fig 4-8. The distribution of full depletion voltage

(2) Leakage current

In general, the leakage current increases by $\sqrt{V}$ before the bias voltage reaches the full depletion voltage and becomes constant after that. But the leakage current of these sensors does not become constant even after the bias voltage reaches the full depletion voltage. This is because the rising of the bias voltage was done quickly (5V/5minutes). It shows a flat behavior if the bias voltage is raised more slowly.

Fig4-9 shows the bias voltage dependence of the leakage current density of 5 sensors. The leakage current density of each sensor with 150V bias voltage is distributed from 1.6nA/cm^2 to 4nA/cm^2 and fully satisfies the specification of <10nA/cm^2 (maximum).

These values are very low in comparison with the present other kinds of silicon strip sensors. Such a low leakage current enables us to screen out even a sensor having few noisy strips by looking at the total leakage current instead of measuring the individual strip currents. Table4-2 summaries the leakage current density of each sensor with 150V.

The value of the leakage current density is corrected at 25°C by using the formula (4.1).

$$\left.\begin{aligned} J_{gen} &= AT^2 \exp\left(-\frac{E}{2k_B T}\right) \\ E &= E_g + 2\left|Et - E_i\right| \quad (=1.2) \end{aligned}\right\} \qquad (4.1)$$

Here, A is a free parameter, E_g is a band gap energy, E_t is a defect level, E_i is a impurity fermi level and T is an absolute temperature.

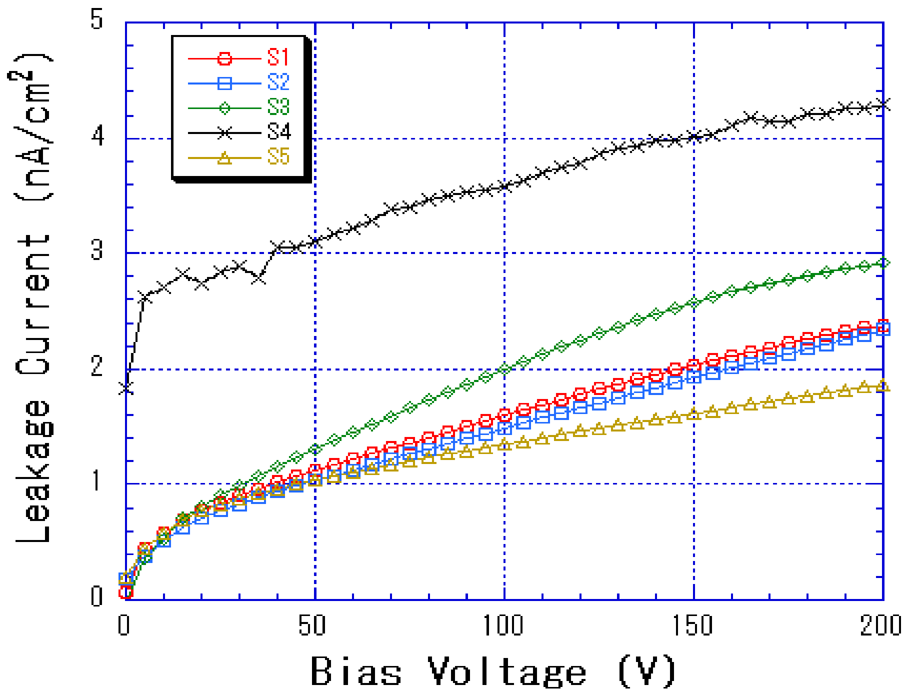

Fig 4-9. Bias voltage dependence of leakage current density at 25°C. The bias voltage was raised by 5V/5min.

Sample	S1	S2	S3	S4	S5	specification
Leakage current density (nA/cm^2)	**2.03**	**1.92**	**2.58**	**4.01**	**1.62**	**< 10** (maximum)

Table 4-2. Leakage current density of 5 sensors with 150V and 25°C.

Fig4-10 shows the distribution of leakage current density of 35 sensors measured by HPK. All sensors satisfy the specification of <10nA/cm^2 (Maximum) and 3nA/cm^2 (average). This histogram includes S1～5. But the value at here is different from at table 4-2. This is due to the difference of the measuring speed. The measuring speed at Hiroshima University was 5V/5min. On the other hand, HPK was measured with 5V/0.5sec since they have to compromise because of the large number of measurements and SSDs. Of course, the slow-measurement is desired.

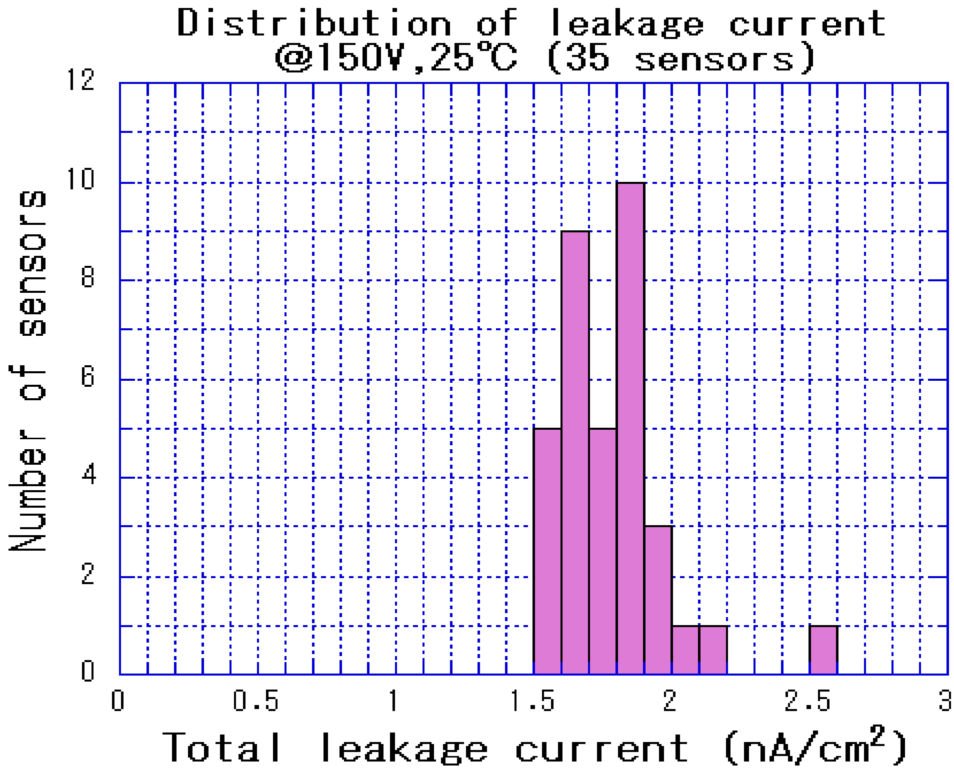

Fig 4-10. The distribution of total leakage current density of 35 sensors

Next, we measured the individual strip currents about one sensor to confirm whether the sensor which satisfies the specification about total leakage current has really few noisy strips. Fig4-11 shows the strip by strip leakage current of one sensor (S4) with 150V bias voltage at 25℃. The value of the leakage current is corrected at 25℃ by using the formula (4.1). The specification of the single strip leakage current is <10nA. It can be seen that there is only one noisy strip. The noisy strip percentage is less than 0.3%. This is not usually considered problem.

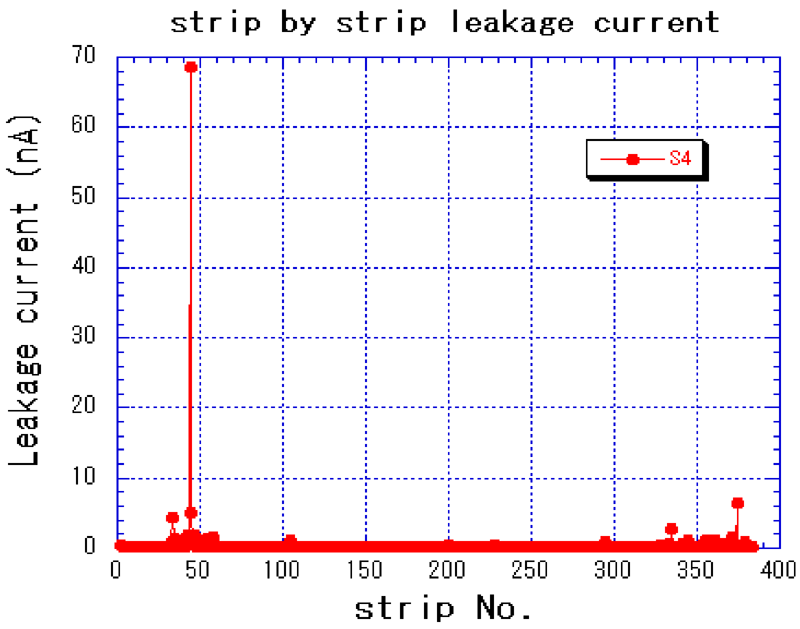

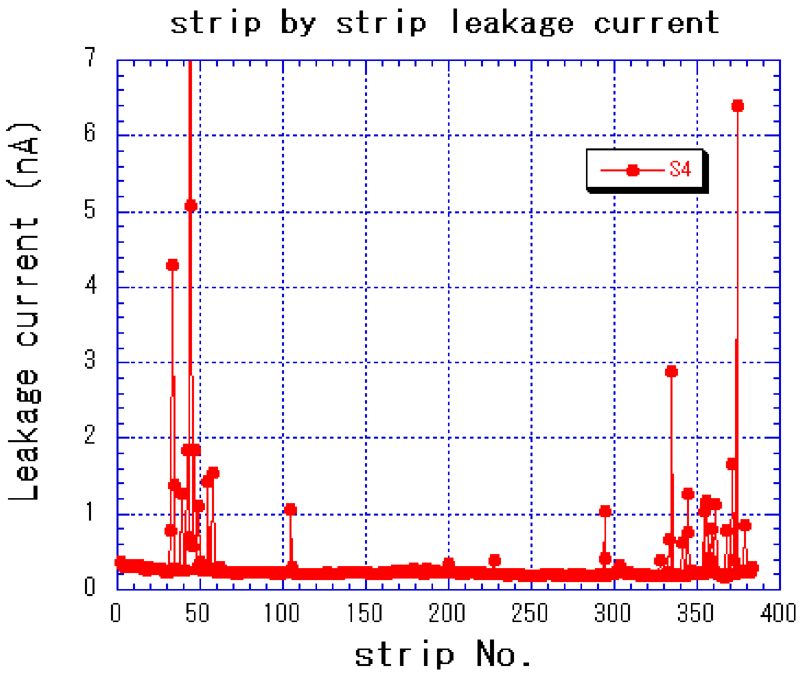

Fig 4-11. Strip by strip leakage current with 150V bias voltage at 25℃.

(3) Coupling Capacitance

Fig4-12 shows the coupling capacitance of 5 sensors and the table4-3 summaries the average of the coupling capacitance of them. The measured strips were only 1,2,3,192, 382,383,384th strips. As one can see, the coupling capacitance of each sensor is about

560pF. This satisfies the specification of >500pF. The larger the strip No. gets, the smaller the value of coupling capacitance is. This is due to the gradient of thickness of SiO_2. Table4-3 summaries the average of the coupling capacitance of each sensor.

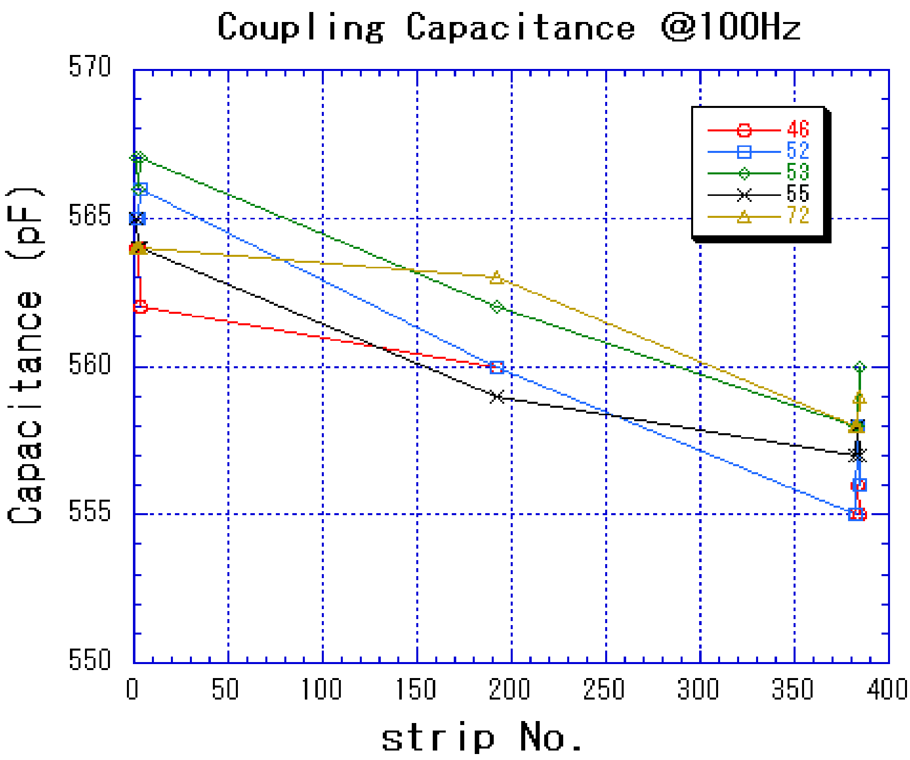

Fig 4-12. The coupling capacitance at 100Hz. The measured strips were only 1,2,3,192, 382,383,384th strips.

Sample	S1	S2	S3	S4	S5	specification
Coupling Capacitance (pF)	**559**	**561**	**563**	**561**	**561**	**>500**

Table 4-3. Coupling capacitance of 5 sensors

(4) Interstrip Capacitance

Fig4-13 shows the interstrip capacitance of 5 sensors. The measured strips were only 2,3,192,382,383th strips. As one can see, the interstrip capacitance of each sensor is about 0.7pF/cm. This satisfies the specification of <1.5pF/cm. For the interstrip capacitance, the capacitance between one strip and its one neighboring strip is dominant. However, over 2 neighboring strips also contribute somewhat too. Thus the interstrip capacitance at the center strip is the largest. Table4-4 summaries the average of the interstrip capacitance of each sensor.

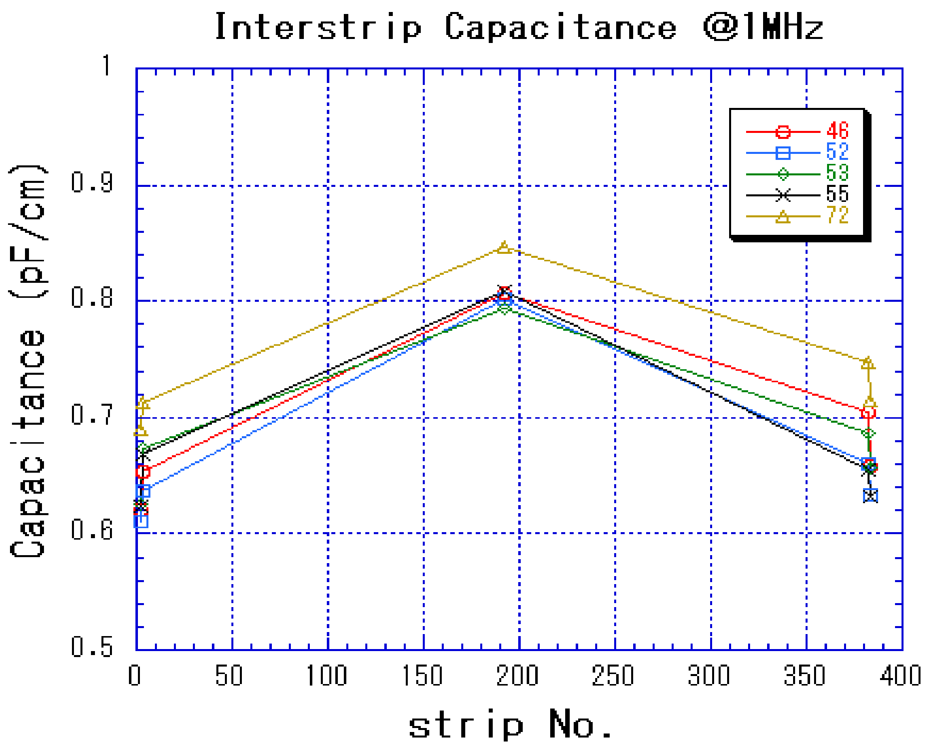

Fig 4-13. Interstrip capacitance of 5 sensors at 1MHz. The measured strips were only 2,3,192,382,383th strips.

Sample	S1	S2	S3	S4	S5	specification
Interstrip Capacitance(pF/cm)	**0.69**	**0.69**	**0.69**	**0.68**	**0.74**	**<1.5**

Table 4-4. The average of the interstrip capacitance. The specification is the value for one strip.

(5) Bias resister resistance

Fig4-14 shows the bias resister resistance of 5 sensors. The measured strips were only 1,2,3,192,382,383,384th strips. The bias resister resistances of each sensor vary from 35 to 59MΩ. This satisfies the specification of 20MΩ < R < 80MΩ. Table4-5 summaries the average of the bias resister resistance of each sensor.

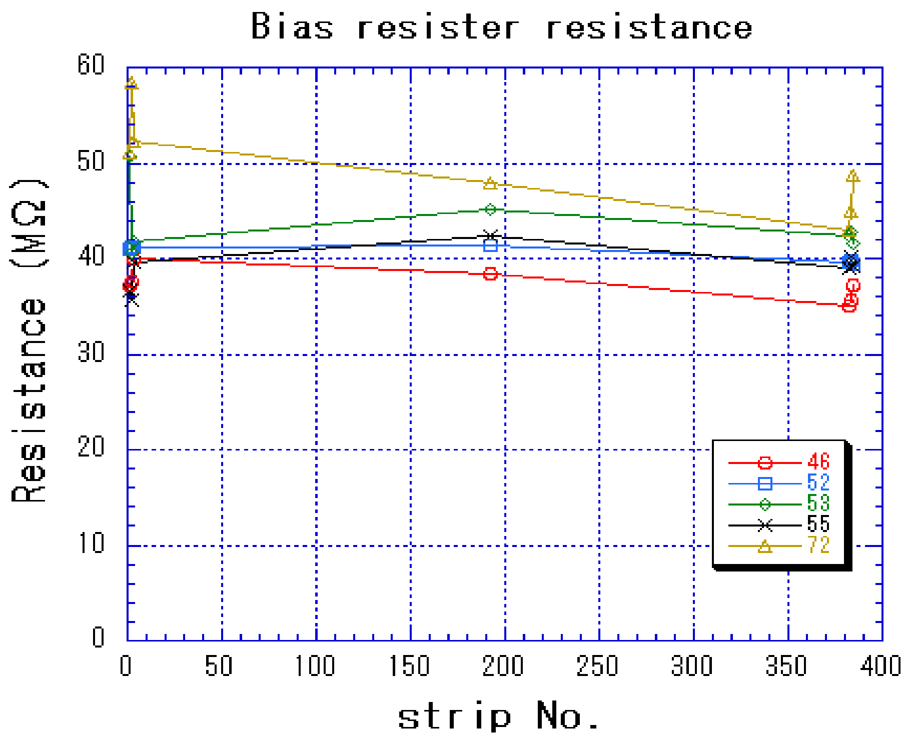

Fig 4-14. Bias resister resistance of 5 sensors.

Sample	S1	S2	S3	S4	S5	specification
Bias resister resistance (MΩ)	**37.3**	**40.5**	**43.6**	**39.0**	**49.5**	**20 < R < 80**

Table 4-5. The average of bias resister resistance. The specification is the value for one bias resister.

(6) Faulted strip rate

In total, there are 13,440 strips on 35 sensors. All strips were inspected at HPK. The total number of faulted strips is only 4 and listed in table4-6 by classifying with failures. The faulted strip rate is less than 0.03% and is extremely small compared to the silicon sensors used in the other experiments. These sensors satisfy the specification of <0.2% enough.

Coupling capacitor(p^+ strip - Al strip) shorts	1
Bias resister is open	3
Al strip is open	0
Bad isolation between neighboring p^+ strips	0
Bad isolation between neighboring Al strips	0
total	4

Table 4-6. The number of faulted strips.

4-2-4. Gamma-ray irradiation

The silicon strip sensors for GLAST is suffers radiation damage by the cosmic-ray in the space and its performance becomes lowers. High-energy particles cause both a surface damage and a bulk damage in the silicon strip sensor. On the other hand, the radiation damage by the gamma-ray is almost only a surface damage. The bulk damage have been so far investigated in detail, thus we investigated the surface damage with gamma-ray.

We examined the radiation damage of the sensor due to gamma-ray from ^{60}Co source to evaluate the fabrication process. The leakage current and the interstrip capacitance were measured before and after gamma-ray irradiation. Another parameters, that is, body capacitance, coupling capacitance and bias resister resistance were not measured because it is thought that they were hardly affected by gamma-ray.

We sampled one sensor (S5) from 5 sensors, which were examined in the previous section, and irradiate it with a dose of 7krad gamma-ray from ^{60}Co source at irradiation facility of the faculty of engineering of Hiroshima University. (We were due to irradiate up to 10krad dose, but we have made the mistake in the estimation for the irradiation time.) The intensity of this ^{60}Co was 370Tbq. The irradiation time was 1620 seconds. This value was estimated by considering the leakage current of the silicon strip sensor during the irradiation, the mass of the sensor (about 7.57g), the energy needed to create an electron-hole pair in the silicon (3.62eV) and so on. The bias voltage was always kept applying to the sensor during the irradiation. Fig4-15 shows the view of the setup for the gamma-ray irradiation.

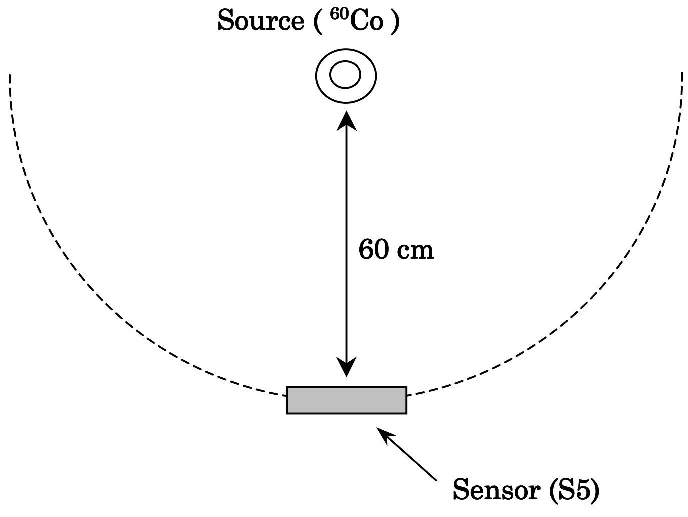

Fig 4-15. The setup for the gamma-ray irradiation

(1) Leakage current

As described in section 2-5, the surface damage occurs at the surface of sensor by gamma-ray irradiation. This damage makes some energy level in the forbidden band and it becomes a cause of the increase of the leakage current.

Fig4-16 shows the bias voltage dependence of the leakage current density for sensor S5 before and after irradiation. The leakage current density of post-irradiation has become about 16 times as large as that of pre-irradiation. The leakage current density with 150V after irradiation is about 30nA/cm^2. The gamma-ray dose of this sensor was 7krad, but this value sufficiently satisfies the specification after 10krad irradiation; <120nA/ cm^2. The value of the leakage current density is corrected for 25℃ by using the formula (4.1).

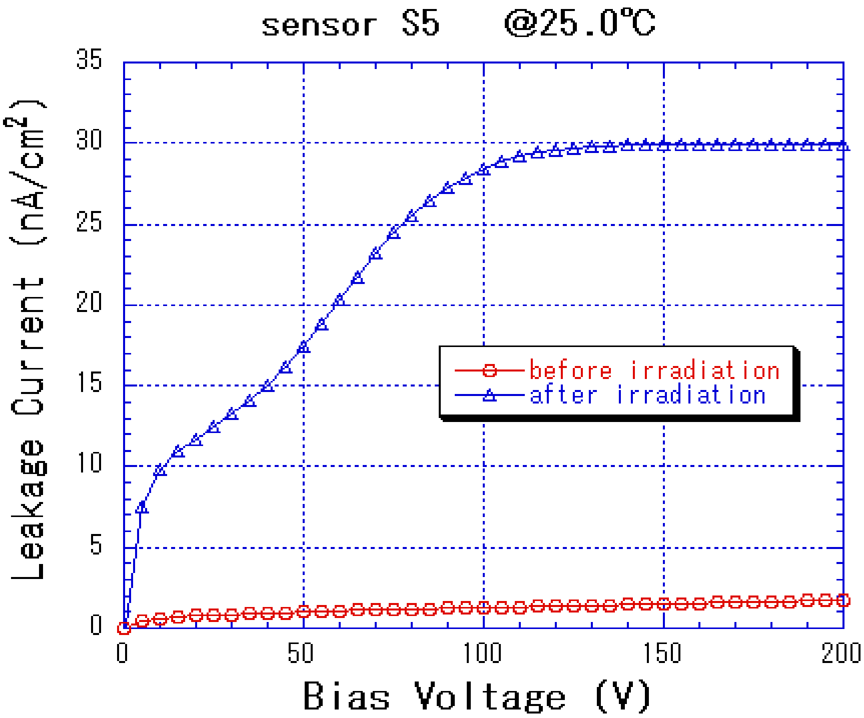

Fig 4-16. The bias voltage dependence of the leakage current density before and after irradiation.

(2) Interstrip capacitance

Fig4-17 shows the interstrip capacitance before and after gamma-ray irradiation. The measured strips were only 2,3,192,382,383th strips. As one can see, there is little difference between pre and post-irradiation. This is in the error tolerance level. The gamma-ray dose of this sensor was 7krad, but this value sufficiently satisfies the specification after 10krad irradiation; <1.6pF/cm.

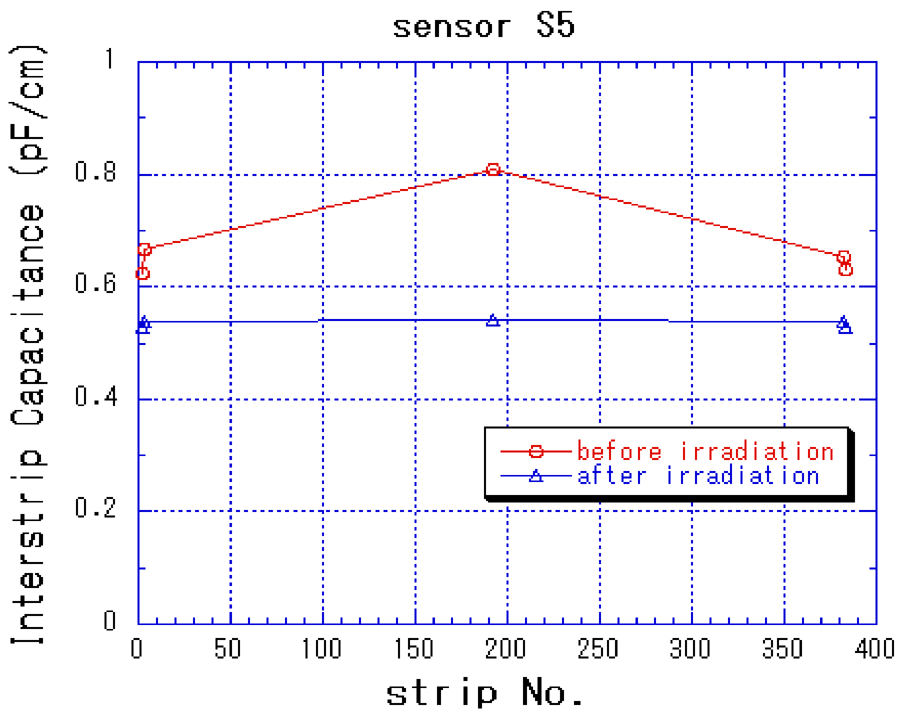

Fig 4-17. Interstrip capacitance before and after irradiation

4-2-5. Conclusion

All sensors satisfy the specification about various parameters, that is, full depletion voltage, leakage current, coupling capacitance, interstrip capacitance and bias resister resistance. The number of faulted strips is only 4 out of 13,440 strips. The faulted strip rate is less than 0.03%.

The specifications about the leakage current and interstrip capacitance after 10krad gamma-ray irradiation are both satisfied. The gamma-ray tolerance of sensors is enough for GLAST mission.

From the above thing, it can be said that these 35 sensors have high quality. As a consequence, it could shift to mass production with the same fabrication process.

4-3. Verifications of Mass Production

As a result of the verification of pre-mass produced sensors (section 4-2), the mass production of sensors has started in Feb. 2001. More than 1,000 SSD have been produced by now, and 622 sensors have been measured in detail. We report their performance verification in the following.

4-3-1. Analysis of the Items

We analyzed the data of the 622 sensors measured by HPK. The measured parameters are as follows.

(1) Full Depletion Voltage
(2) Leakage Current
(6) Faulted Strip Rate

The measuring methods and its set up of these parameters are identical to ones in section 4-2 except for the temperature during the measurement. It was kept constant at 25℃.

4-3-2. Results

(1) Full Depletion Voltage

The bias voltage dependence of the bulk capacitance was measured for all sensors by HPK. Some examples of C-V curves are shown in Fig4-18. Here, the inverse square of the bulk capacitance is plotted to allow an easier determination of the full depletion voltage. The distribution of full depletion voltage for 622 sensors is shown in Fig4-19. As one can see, the full depletion voltage spreads from 40V to 130V. All sensors satisfy the specification of <120V except for one sensor. These full depletion voltage is relatively low for 410 μm thick silicon sensor and is due to the use of high resistivity wafer (5kΩ cm). The reason why the full depletion voltage scatters so widely is due to the difficulty in controlling the resistivity of wafer at high value.

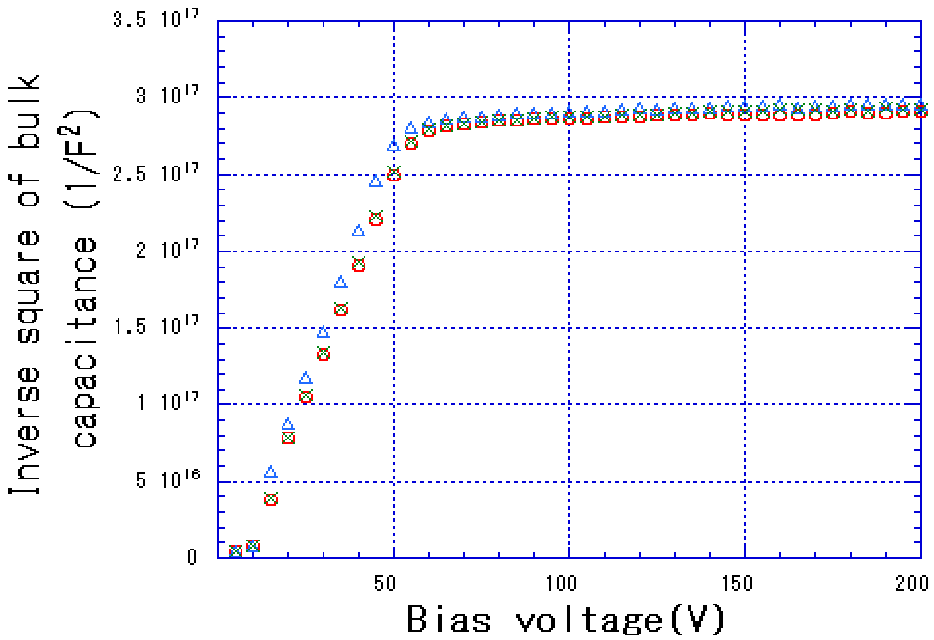

Fig 4-18. The bias voltage dependence of bulk capacitance. The plot is the inverse square of the bulk capacitance.

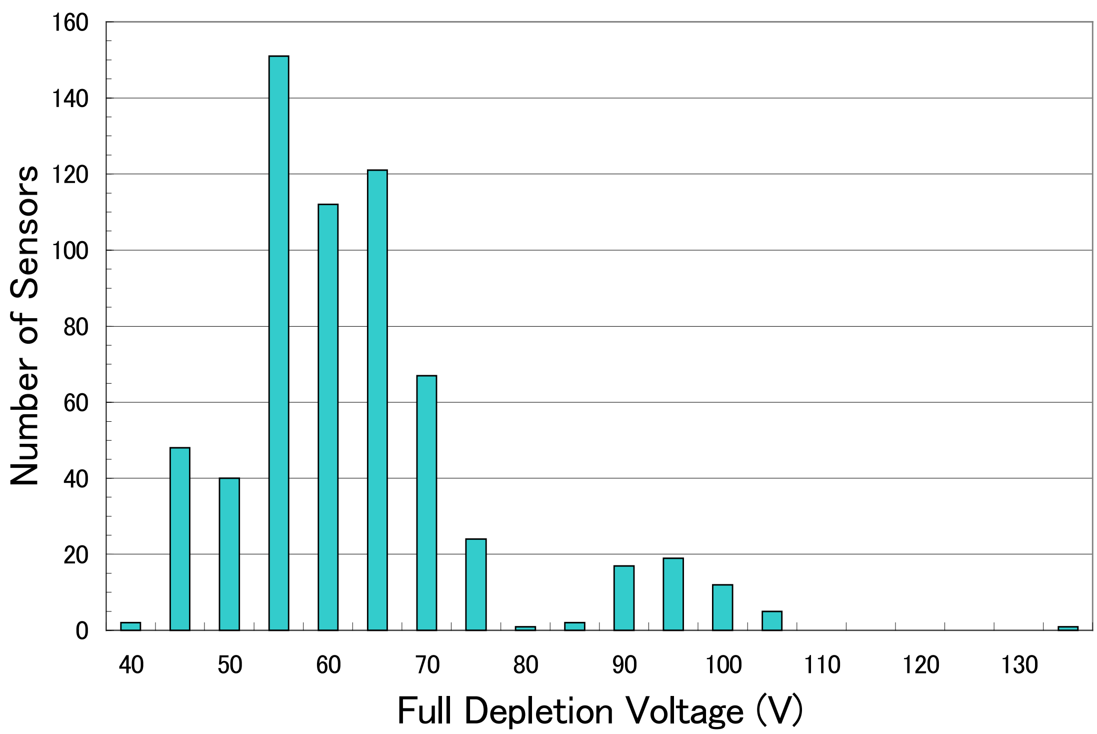

Fig 4-19. The distribution of the full depletion voltage for 622 sensors.

(2) Leakage Current

The bias voltage dependence of the leakage current was measured for all sensors at HPK. Some results of the measurement are plotted in Fig4-20 for the same sensors plotted in Fig4-18. It can be seen that the leakage current of these sensors does not become constant even after the bias voltage reaches the full depletion voltage. This is because the rise of the bias voltage was done quickly (5V/0.5sec). It shows a flat behavior if the bias voltage is raised very slowly, but they have to compromise because of the large number of measurements and SSDs.

Fig4-21 shows the distribution of the leakage current density for 622 sensors with 150V bias voltage. The average leakage current density of these sensors is 2nA/cm^2. This satisfies the specification of 3nA/cm^2 (average) enough. This value is very low in comparison with present other kinds of silicon strip sensors and indicating a very mature fabrication process. Such a low leakage current enables us to screen out even a sensor having few noisy strips by looking at the total leakage current instead of the individual strip currents.

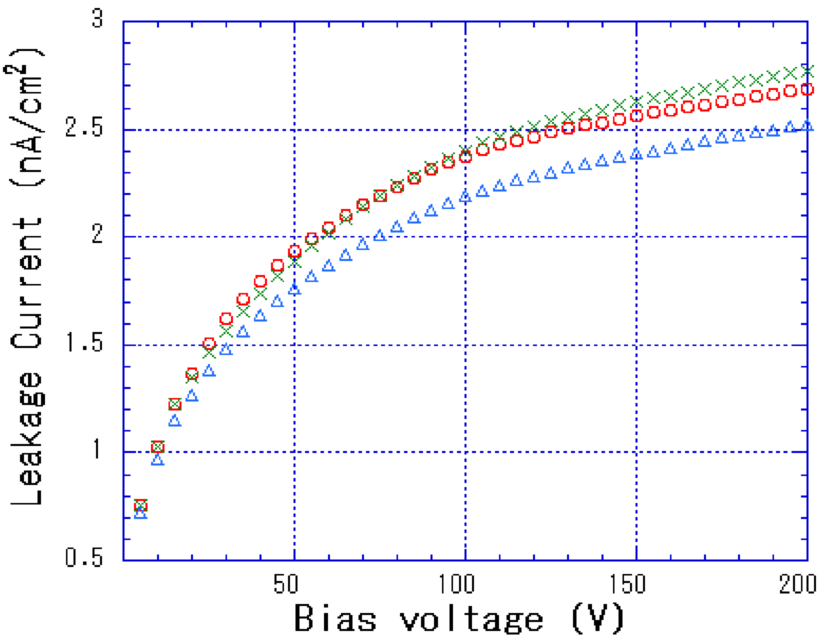

Fig 4-20. The bias voltage dependence of the leakage current density at 25℃. These sensors are the same ones plotted in Fig4-18.

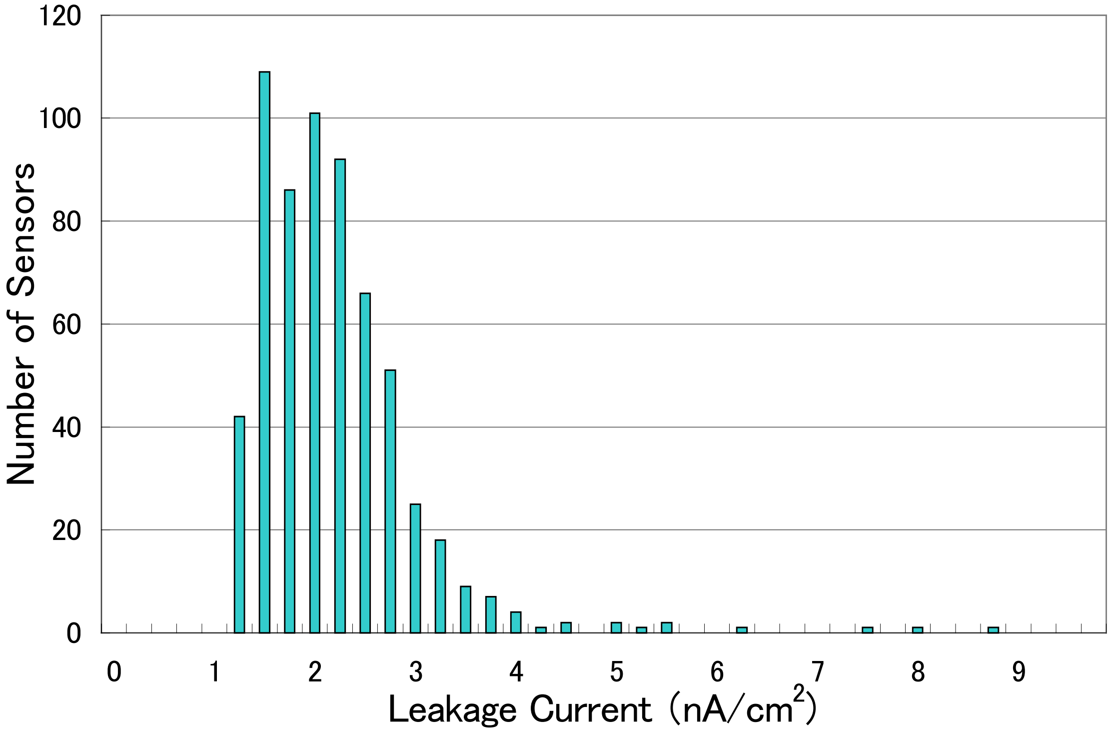

Fig 4-21. The distribution of the leakage current density with 150V bias voltage at 25°C.

(3) Faulted Strip Rate

In total, there are 237,676 strips on 622 sensors. All strips were inspected at HPK. The total number of faulted strips is only 19 and listed in table4-7 by classifying with failures. The faulted strip rate is less than 0.01% and is extremely small compared to the silicon sensors used in the other experiments. These sensors satisfy the specification of <0.2%.

Coupling capacitor(p^+ strip - Al strip) shorts	11
Bias resister is open	5
Al strip is open	0
Bad isolation between neighboring p^+ strips	3
Bad isolation between neighboring Al strips	0
total	19

Table 4-7. The number of faulted strips.

4-3-3. Gamma-ray Irradiation

We examined the radiation damage of sensors in addition to the analysis mentioned in previous section, by irradiating the gamma-ray with ^{60}Co source to evaluate the fabrication process that effects the radiation tolerance.

The "test sensors" are used for this irradiation to save the "full size sensors" for the Flight-Model (FM). The test sensors are fabricated on the wafer on which the full size sensors are fabricated. They are fabricated with the same process and have the same layout except for the strip number. Thus if there is a problem with the fabrication of the full size sensor, the same problem is expected to be found in the test sensor. The strip number of the test sensor is 8, while the number of the full size sensor is 384. The picture of these sensors on the 6-inch wafer is shown in Fig3-4.

We sampled one test sensor from every production lot of about 30 full size sensors. The test sensors were irradiated up to the 10krad dose at the irradiation facility of the faculty of engineering of Hiroshima University. The irradiation time was estimated by considering the leakage current of the silicon strip sensor in the past measurement and the half-life of ^{60}Co (5.27y). The test sensors were biased during irradiation with 150V. After the irradiation, the test sensors were kept at 20 ℃ and also biased with 150V. The leakage current, interstrip capacitance and interstrip resistance were measured before and after irradiation.

(1) Leakage Current

The bias voltage dependence of the leakage current for the test sensors was measured before gamma-ray irradiation. The measuring method and its set up is identical to one in section 4-2. The temperature was kept constant at 20℃ during the measurement.

After gamma-ray irradiation, the bias voltage was always kept applying to the sensors except for 1 hours to carry the sensors from irradiation facility to our laboratory. The leakage current was measured a week after the irradiation in the same way as before irradiation.

Fig4-23 shows the leakage current density before and after irradiation with 150V bias voltage at 25℃. The value of the leakage current is corrected at 25℃ by the formula (4.1). The average leakage current density before irradiation is about 5nA/cm^2. On the other hand, the leakage current density a week after irradiation is about 70nA/cm^2. This value satisfies the specification of <120nA/cm^2 for after 10krad irradiation.

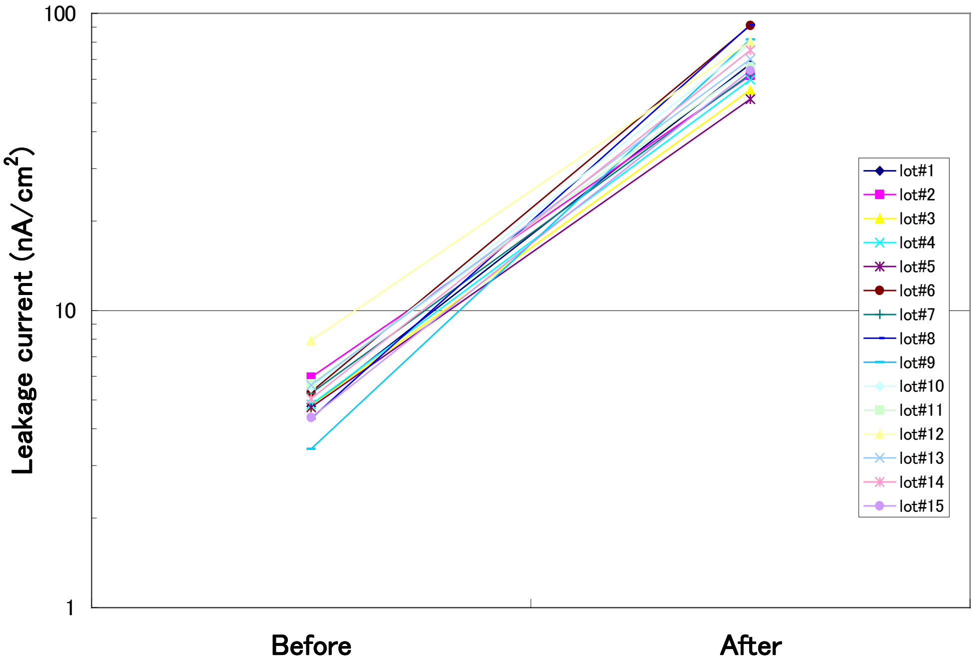

Fig 4-23. The leakage current density of the test sensors before and after the irradiation at 25℃.

(2) Interstrip Capacitance

The interstrip capacitance of the test sensors was measured for all strips before gamma-ray irradiation. The measuring method and its set up is identical to one in section 4-2. The measurement after irradiation was done a week after the irradiation in the same way as pre-irradiation.

In total, there are 8 strips in the test sensor and we measured for 6 strips which can be measured (6 strips) before and after the irradiation. Since the interstrip capacitance is the capacitance between one strip and its neighbors, 2 strips (1,8th strip) located in the endmost can not be measured. The results are shown in Fig4-24 where the average of 6 strips is plotted. There is no significant difference between before and after the irradiation. These values satisfy the specification of <1.5pF/cm (before irradiation) and <1.6pF/cm (after 10krad irradiation), respectively.

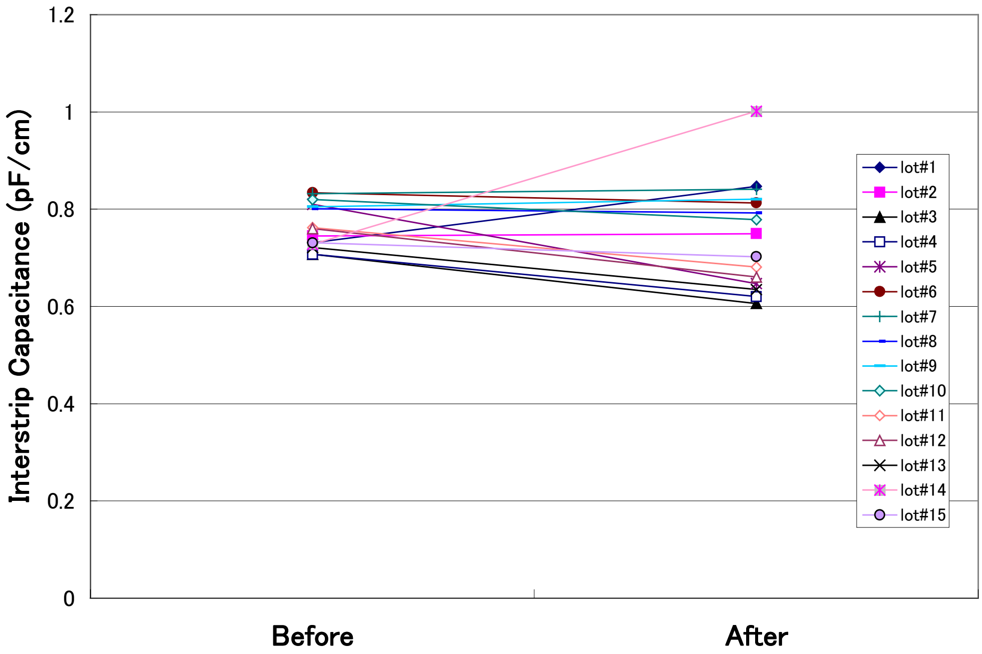

Fig 4-24. The interstrip capacitance of test sensors before and after the irradiation.

(3) Interstrip Resistance

Fig4-25 shows the set up for the measurement of interstrip resistance. The 10V bias voltage is applied to the test sensors. In this set up, if there is no problem with the interstrip resistance, the measured resistance is the one of bias resister. The results are shown in table4-8. Here, the "lot" is the production unit and its number indicates the order of production.

The interstrip resistance of the full size sensors was measured with non-irradiated and that of the test sensors was measured before and after the irradiation. In the full size sensor, there are only 2 points, that is, 4 strips below 1GΩ out of 180k strips. On the other hand, there was one bad isolation point, that is, 2 strips in one test sensor with lot-7 before irradiation. The interstrip resistance for this point was 781.3kΩ. After the irradiation, the interstrip resistance for this point has got worse further and its value is 77.6kΩ. In addition to this point of this test sensor, the isolation at two points have got worse after the irradiation. The value of interstrip resistances for these points are 10.1kΩ and 60.7kΩ, respectively. It is not a problem that the only 2 strips are below 1GΩ.

There is a correlation between full size sensors and test sensors. The lot number of the full size sensor which has bad isolation point and that of the test sensors where the bad isolation points have appeared after the irradiation is same or close in value.

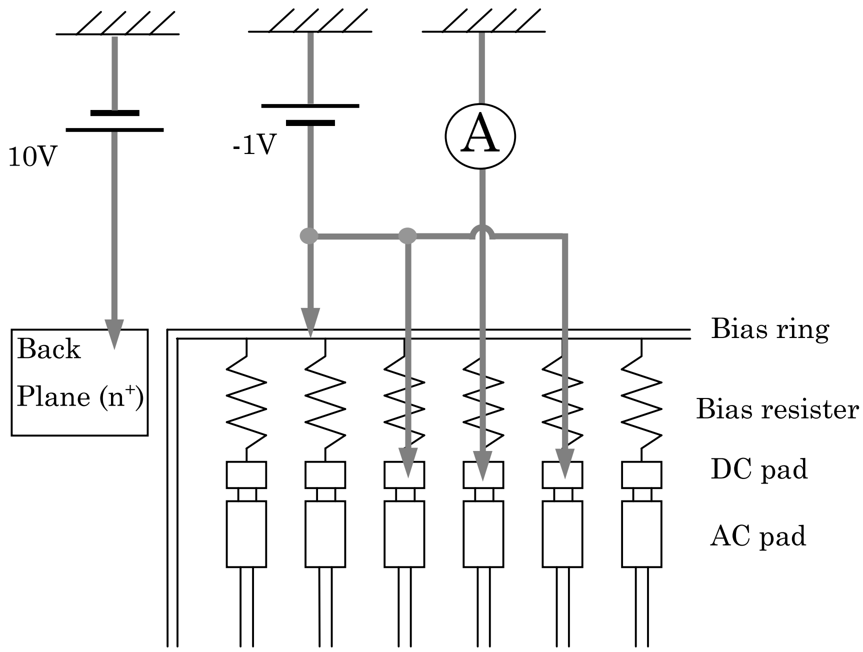

Fig 4-25. The set up for the measurement of interstrip resistance.

Lot No.	Full size sensors -Non-irradiated-	Test sensors -before irradiation-	Test sensors -after irradiation-
1	0/12672	0/8	0/8
2	0/14592	0/8	0/8
3	0/10368	0/8	0/8
4	0/11520	0/8	0/8
5	0/11904	0/8	0/8
6	0/13824	0/8	2/8 (10.1kΩ)
7	4/10752	2/8 (781.3kΩ)	2/8 (77.6kΩ)
8	0/9984	0/8	2/8 (60.7kΩ)
9	0/10752	0/8	0/8
10	0/13440	0/8	0/8
11	0/10368	0/8	0/8
12	0/12288	0/8	0/8
13	0/14208	0/8	0/8
14	0/10368	0/8	0/8
15	0/16512	0/8	0/8

Table 4-8. The number of strips where the interstrip resistance is below 1GΩ out of the total number of strips and its resistance. In this measurement, one bad isolation point results in the 2 bad isolation strips. The value of resistance above is the one between 2 bad isolation strips.

4-3-4. Conclusion

We have investigated the 622 sensors for GLAST FM sensor. The full depletion voltage distributes from 40V to 130V and the average was 60V. These values are relatively low for 410 μm thick silicon sensor and is due to the use of high resistivity wafer (5kΩcm). The average leakage current density of these 622 sensors with 150V bias voltage at 25℃ is about $2nA/cm^2$. This value is very low in comparison with present other kinds of silicon strip sensors, indicating a very mature fabrication process. The number of faulted strips is 19 out of 237,676, i.e. the faulted strip percentage is less than 0.01% and they affect only 2% of the tested 622 full size sensors. All 622 sensors satisfy its specifications except for one sensor.

We also examined the radiation tolerance of sensors using the ^{60}Co gamma-ray source. Due to the irradiation of 10krad gamma-ray, the leakage current density of test sensors increased from $5nA/cm^2$ to $70nA/cm^2$. This value satisfies the specification of $<120nA/cm^2$ for after 10krad irradiation. The interstrip capacitance of the test sensors did not change significantly between before and after the irradiation. This also satisfies the specification for after irradiation. In the interstrip resistance, there is a correlation between non-irradiated full size sensors and test sensors before and after irradiation. The lot number of the full size sensor, which has bad isolation point, and that of the test sensors where the bad isolation points have appeared after the irradiation, are the same or close in value. It is not usually considered to be a problem that the only 2 points, that is, 4 strips are below 1GΩ. But the radiation tolerance of full size sensors with lot 6～8 needs to be investigated.

Chapter 5
Extensive Study of Radiation Damage of Low-leakage current Sensors

The leakage current density of silicon strip sensors for GLAST is about $2nA/cm^2$ at 25°C. This value is comparable to a low-leakage current photodiode. This kind of low-leakage current sensor did not exist in the past. We thus investigated the radiation damage of these low-leakage current sensors because there might be unknown phenomena. First of all, we investigated the relation between the gamma-ray dose and increase of the leakage current. This is reported in section 5-1. Then we investigated the effect of the bias voltage to the sensor for the radiation damage. This is reported in section 5-2. The test sensors of GLAST are used for this investigation in order to save the full size sensors which must be used for the Flight-Model (FM).

5-1. Leakage current vs. Gamma-ray dose

We sampled 12 test sensors from one production lot of about 30 full size sensors and irradiated them with a dose of 1k, 3k, 10k, 20k, 25k or 50krad gamma-ray from ^{60}Co source, so that two test sensors were irradiated with the same dose.

The time dependence of the leakage current for the test sensors was measured after the gamma-ray irradiation. The 150V bias voltage was always kept applying to the sensors during and after the irradiation. Here, Al electrodes were electrically floating. The temperature was kept constant at 20°C during the measurement. Fig5-1 shows the time dependence of the leakage current density after irradiation with 150V bias voltage at 20°C.

The leakage current increased with gamma-ray dose as we had expected. But, as one can see, the relation between the gamma-ray dose and the leakage current is not linear. We plotted the dose dependence of the leakage current density one month (720 hours) after the irradiation in Fig5-2. Here, the plotted leakage current density is the average of two sensors which are irradiated with the same dose. We fitted this plot with a function of $y=A+Bx^C$ (x : gamma-ray dose). As one can see, the leakage current density is proportional to the 0.8th power of dose.

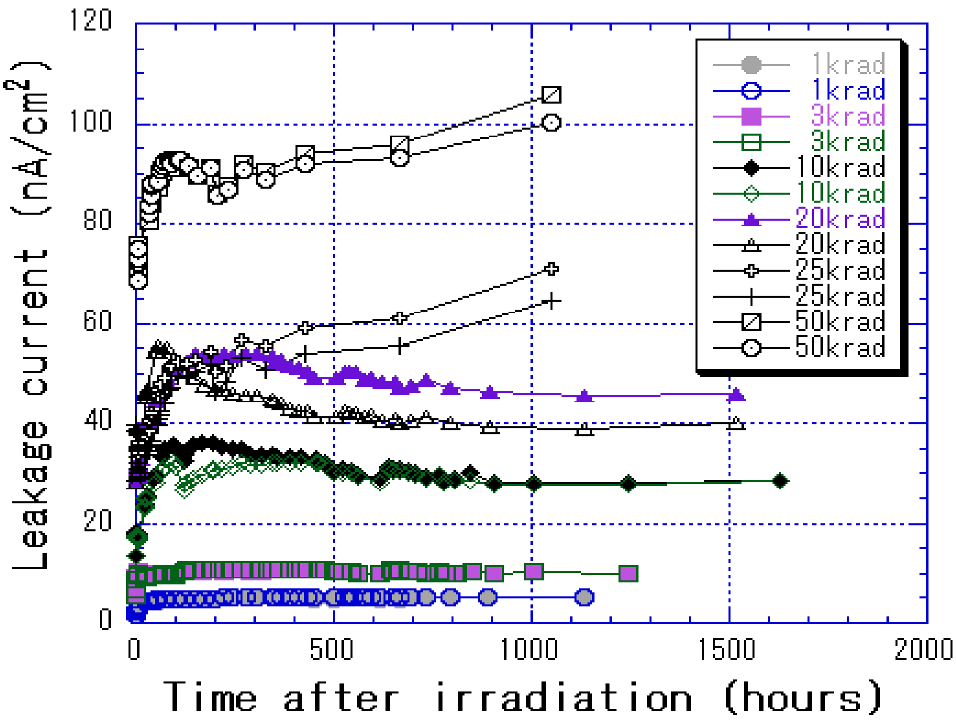

Fig 5-1. The time dependence of the leakage current density with 150V bias voltage at 20°C.

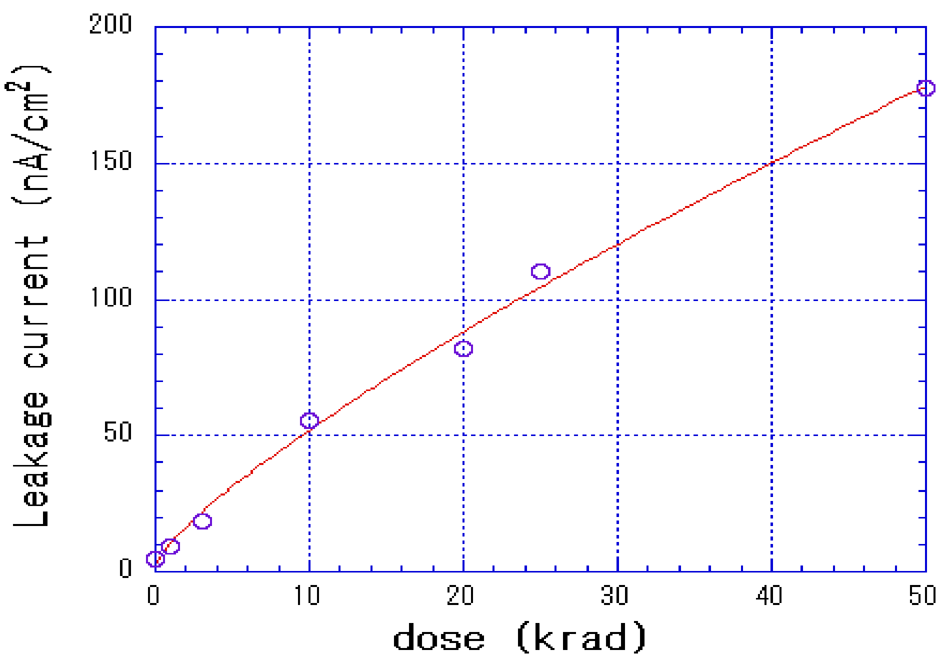

Fig 5-2. Gamma-ray dose vs. leakage current density at 20℃ one month (720 hours) after the irradiation.

5-2. The effect of the bias voltage

The behavior of the leakage current after the irradiation is related to the bias voltage to the sensor during and after the irradiation [12]. In order to investigate this phenomenon in more detail, we performed the following measurement.

The 7 test sensors were sampled from one production lot which is the same one investigated in section 5-1. These test sensors were irradiated up to the 10krad gamma-ray dose with ^{60}Co source. The time dependence of the leakage current for the 7 test sensors was measured after the irradiation.

During the irradiation, the 150V bias voltage was applied to one sample out of 7 samples. This one sample was kept applying the bias voltage after the irradiation. This one sample is represented by “on” in Fig5-3. The other 5 samples were biased with 150V at 7 minutes, 3 hours, 1 days, 3 days and 10 days after the irradiation, respectively. These samples are represented by “7 minutes after”, “3 hours after”, “1 day after”, “3 days after” and “10 days after” in Fig5-3, respectively. The remainder one was not applied the bias voltage during and after the irradiation except for 10 seconds during the measurement. This sample is represented by “off” in Fig5-3. After the irradiation, the samples were kept at 20℃. Fig5-3 shows the time dependence of the leakage current after the irradiation with 150V bias voltage at 20℃.

The leakage current of the sample, which was kept applying the bias voltage during and after the irradiation, increased with time and became constant conclusively. This phenomenon is also perceived from the result of section 5-1. On the other hand, the leakage current of the test sensors, which were not applied the bias voltage during the irradiation, showed the irregular behavior before the bias voltage was applied to them. After the bias voltage was applied to them, the leakage current of these sensors initially increased. After that, the leakage current gradually decreased and became constant.

There is a significant difference in the leakage current between the test sensor, which was kept applying the bias voltage during the irradiation, and the other sensors. The ultimate value of the leakage current of the former is about twice as large as that of the latter. The bias voltage is always kept applying to the silicon strip sensor for the GLAST mission, thus it must be kept applying to the silicon strip sensor during and after the irradiation when one estimates the surface damage of GLAST sensor. Moreover, the bias voltage must be kept applying to the sensor for a long time in order to stabilize the leakage current of the sensor after the irradiation.

In addition to them, it can be seen that there is an effect which softens the radiation damage (annealing effect) when the bias voltage is kept applying to the post-irradiated sensor which were not applied the bias voltage during the irradiation. Moreover, when we applied the bias voltage earlier after the irradiation, the effect was larger. As mentioned in section 5-2, the mechanism of the annealing effect is explained in such a way that holes trapped in the SiO_2 recombine with electrons in the n-bulk through the tunneling effect. We guess that this phenomenon mentioned above is due to the increase of the tunneling probability for a certain cause. However, the cause is not solved well yet.

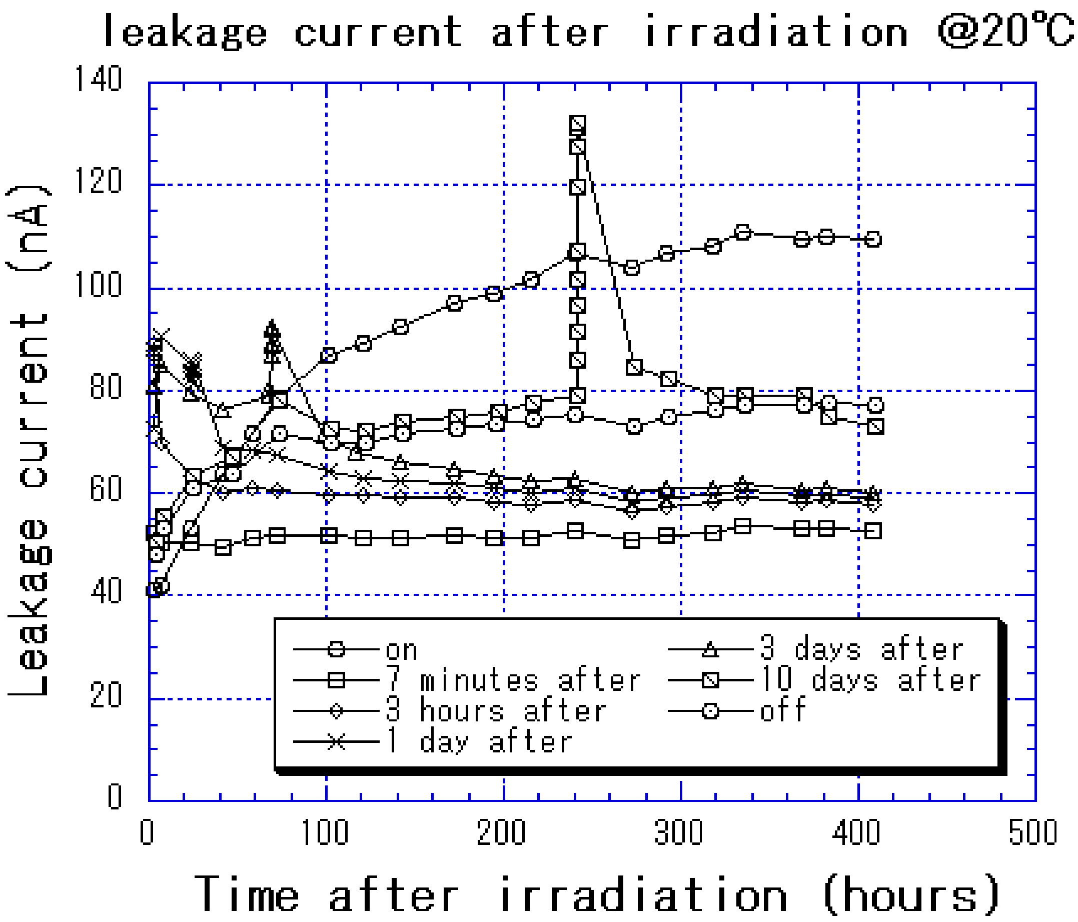

Fig 5-3. The time dependence of the leakage current with 150V bias voltage at 20°C.

5-3. Conclusion

We investigated the relation between the gamma-ray dose and increase of the leakage current. The leakage current of the irradiated sensor increases as the 0.8th power of dose.

Next, we investigated the effect of applying the bias voltage during the irradiation.

The leakage current significantly differed whether the bias voltage was applied during the irradiation or not. The ultimate value of the leakage current of the former is about twice as large as that of the latter. Thus, it must be kept applying to the silicon strip sensor during and after the irradiation when one estimates the surface damage of GLAST sensor. Moreover, the bias voltage must be kept applying to the sensor for a long time in order to stabilize the leakage current of the sensor after the irradiation.

It can be seen that there is an effect which softens the radiation damage (annealing effect) when the bias voltage is applying to the post-irradiated sensor which were not applied the bias voltage during the irradiation. Moreover, if we applied the bias voltage earlier after the irradiation, the effect is larger. We explain that this phenomenon is due to the increase of the tunneling probability for a certain cause. However, the cause of this phenomenon is not well understood yet, and has to be investigated in detail in the future.

Acknowledgement

I would like to express my thanks to Prof. T. Ohsugi for his continual support. Special thanks are due to Prof. Y. Fukazawa for his encouragement and support. I express my thanks to Dr. S. Yoshida and Dr. Y. Iwata for their continual support and guidance on my study.

The gamma-ray irradiation was performed at the ^{60}Co Irradiator of Radiation Research Facility, the Faculty of Engineering of Hiroshima University. I would like to express special thanks to Prof. N. Ohta for his kind help to perform the irradiation.

I acknowledge Mr. H. Mizushima, S. Ogata and K. Yamanaka for their useful discussion. I wish to thank all of the members of my laboratory for their continuous help.

References

[1] ‘Science expected with GLAST’, Japan GLAST Working Group,1997

[2] T. Graves, ‘URL : http://www-glast.stanford.edu/’, 2000

[3] William R. Leo, ‘Techniques for Nuclear and Particle Physics Experiments’, Second Revised Edition, Springer-Verlag, 1994

[4] H. Kitabayashi, ‘Surface Damage of AC-coupled Silicon Microstrip Sensors by γ-rays’, Graduation Thesis, Hiroshima University, 1996

[5] M. Ikeda, ‘Performance of Large Size Silicon Strip Sensor Fabricated by 6-inch Process’, Master Thesis, Hiroshima University, 1999

[6] T. Ohsugi et al. Nucl. Instr. And Meth. A-265 (1988) 105

[7] Ohsugi et al., ‘Design optimization of radiation-hard, double-sided, double-metal, AC-coupled silicon strip sensors

[8] S. Worm, ‘Radiation effects in double-sided silicon sensors for CDF’, Nucl. Instr. And Meth. A-418 (1998) 120-127

[9] T. Ohsugi et al., ‘Design optimization of radiation-hard, double-sided, double-metal, AC-coupled silicon sensors’, Nucl. Instr. And Meth. A-436 (1999) 272-280

[10] H. Sadrozinski, ‘GLAST LAT Silicon Strip Detector (SSD) Prototyping Process and Status’, GLAST LAT TECHNICAL DOCUMENT, LAT-TD-00142-01, 2001

[11] S. Yoshida et al., ‘Heavy ion irradiation on silicon strip sensors for GLAST’, 2001 IEEE

[12] K. Yamanaka, ‘Radiation Damage Experiment of Large Area Silicon Strip Sensors for GLAST’, Graduation Thesis, Hiroshima University, 2000

[13] J. Miyamoto, G.F. Knoll, 'The statistics of avalanche electrons in micro-strip and micro-gap gas chambers', Nucl. Instr. And Meth. A-399 (1997) 85-93

[14] T. Ohsugi et al., 'Micro-discharge at strip edge of silicon microstrip sensors', Nucl. Instr. And Meth. A-383 (1996) 116-122

[15] T. Ohsugi et al., 'Micro-discharge noise and radiation damage of silicon microstrip senosrs', Nucl. Instr. And Meth. A-383 (1996) 116-173

[16] H. Sadrozinski, 'The GLAST instrument, a gamma-ray large area space telescope', Nucl. Instr. And Meth. A-419 (1998) 300-305

[17] D. Tournear, 'The silicon tracker for the GLAST large area space telescope', Nucl. Instr. And Meth. A-473 (2001) 61-66

[18] J.F. Krizmanic, 'GLAST: The Gamma-ray Large Area Space Telescope', Nucl. Instr. And Meth. A-418 (1998) 161-172